LASER BIOEFFECTS RESULTING FROM NON-LINEAR INTERACTIONS OF ULTRASHORT PULSES WITH BIOLOGICAL SYSTEMS

Final Report
AFOSR Grant F49620-01-1-0211

Randolph D. Glickman, Ph.D., P.I.

Department of Ophthalmology
University of Texas Health Science Center at San Antonio
San Antonio, Texas

Grant Period: 1 April 2001 to 14 July 2004

TABLE OF CONTENTS

Laser Bioeffects Resulting from Non-Linear Interactions of Ultrashort Pulses with Biological Systems

Final Report
AFOSR Grant F49620-01-1-0211

Randolph D. Glickman, Ph.D.
Department of Ophthalmology
University of Texas Health Science Center at San Antonio
San Antonio, Texas

Summary

The original goal of this project was to determine the role of non-linear interactions underlying the bioeffects induced by ultrashort pulse laser pulses. As initially conceived, this line of investigation was to be principally directed at understanding the contribution of multiphoton absorption. This indeed was a major focus of the research project, but for various reasons the scope of the work was expanded to include identification of the intracellular mechanisms that determine the cellular response to the absorption of optical radiation, and to develop and implement a non-invasive means for measuring the thermal gradients induced by the absorption of laser radiation in tissue. Both of these ancillary projects were successful in that (1) the transcription factor NF-B was found to be activated by visible laser exposure in a way that appeared to be dependent on the absorption of laser energy in the melanin granules of the retinal pigment epithelial cell, and (2) by exploiting the temperature-dependent nature of the proton resonance frequency (PRF), magnetic resonance thermography was successfully used to measure temperature gradients induced in tissue phantoms during laser exposure, and these gradients closely followed the spatial distributions predicted by classical heat diffusion theory.

In the area of non-linear tissue interaction mechanisms, laser-induced breakdown has the lowest energy threshold in the femtosecond domain, and is responsible for production of threshold ocular lesions. It has been proposed that multiphoton absorption may also contribute to ultrashort-pulse tissue damage, based on the observation that 33 fs, 810 nm pulse laser exposures caused more DNA breakage in cultured, primary RPE cells, compared to CW laser exposures delivering the same average power. DNA breakage was assessed with single cell gel electrophoresis, i.e. the "comet" assay. Subsequent studies, demonstrating two-photon excitation of fluorescence in isolated RPE melanosomes, appeared to support the role of multiphoton absorption, but mainly at suprathreshold irradiance. Additional experiments, however, did not show a consistent difference in the DNA strand breakage produced by ultrashort and CW threshold exposures. DNA damage appeared to be dependent on the amount of melanin pigmentation in the cells, rather than the pulsewidth of the laser; current studies have found that, at threshold, CW and ultrashort pulse laser exposures produced almost identical amounts of DNA breakage. A theoretical analysis suggested that the number of photons delivered to the RPE melanosome during a single 250 fsec pulse *at the ED_{50} irradiance* is insufficient to produce multiphoton excitation. This result appeared to exclude the melanosome as a locus for two- or three-photon excitation; however, a structure with a larger effective absorption cross-section than the melanosome may interact with the laser pulses. One

possibility is that the nuclear chromatin acts as a unit absorber of photons resulting in DNA damage, but the near equivalence of the comet assay results, in RPE cells exposed to ultrashort and CW laser, indicates that multiphoton absorption is not a major contributor to the ultrashort pulse laser damage threshold in the near infrared (but is likely to contribute to suprathreshold tissue damage).

The response of biological cells to laser radiation is the result of a complex series of interactions. The cells of the retinal pigment epithelium (RPE) are subject to photo-oxidative stress arising from the interaction of incident light with lipofuscin, melanin, and other pigment granules in the RPE cytoplasm. Specific genotypic responses to these stressors are controlled by transcription factors, such as NF-κB (RelA/p50 dimer). The effect of CW laser exposures on NF-κB nuclear translocation have been studied in a line of human-derived RPE cells (hTERT-RPE) that develop melanin pigmentation in culture. The cells were exposed to the CW emission of an Argon-ion laser for 10 m at 0.5 W/cm2, a range previously shown to produce oxidation of cellular proteins, DNA, and antioxidants. NF-κB dimer was measured in nuclear extracts by an electrophoretic mobility shift assay. NF-κB nuclear translocation exhibited a modest, early peak at 1 h, and a larger, late peak at 24 h. NF-κB activation could be reduced only by some antioxidants; for example, 20 mM N-acetyl-L-cysteine or 100 μM pyrrolidine dithiocarbamate were ineffective, while 500 μM ascorbic acid was highly effective. These results indicate that interaction of the laser with the RPE melanin granules is a likely source of oxidative reactions, and the induction of photoxidative stress activates NF-κB, but it remains to be determined if NF-κB is pro- or anti-apoptotic in the RPE cell.

An important component of laser-tissue interaction is the production of thermal stress in the radiated tissue. The possibility to induce selective hyperthermia in a target tissue or organ is of great interest for the treatment of cancer and other diseases, however, the therapy is currently limited because the temperature required for optimal tissue response is unknown, and the ability to perform accurate thermography in the radiated tissue may be limited. To overcome this limitation, we implemented a non-invasive thermographic method and validated it by measuring laser-induced temperature gradients in an ocular tissue phantom. Magnetic resonance thermography (MRT) was used as a non-invasive method to determine the temperature distribution inside the phantom during exposure to a continuous wave diode laser at 806 nm wavelength with 1 watt maximum output. The laser beam had a quasi-gaussian profile, with a radius of 0.8-2.4 mm at the target. High quality temperature images were obtained from temperature-dependent phase shifts in the proton resonance frequency with a resolution of 1deg C or better, using a 2T magnet. A phantom with a layer of bovine RPE melanin of 1.5 mm thickness was used to determine the spatial resolution of the MRT measurements. Three dimensional temperature maps were also constructed showing a spatial resolution of 0.25 mm in all directions. The heat distribution depended on the laser parameters, as well as the orientation of the melanin layer with respect to the incident laser beam. The temperature profiles determined by MRT closely followed predictions of a heat diffusion model, based on the optical properties of infrared light in melanin. These results support the use of MRT to map temperature gradients in a small organ such as the eye, as well as to validate models of laser-induced thermal tissue damage.

SECTION ONE

Multiphoton Absorption and Ultrashort Pulse Laser Bioeffects in the Retinal Pigment Epithelium

INTRODUCTION

Multiphoton absorption

The possibility of multiphoton absorption was first hypothesized by Goppert-Mayer in 1931, who proposed a mechanism by which photons absorbed within a sufficiently short time window, i.e. $\leq 10^{-18}$ sec, could cumulatively add their energy to a chromophore, exciting it to an energy level approximately twice as great as that of the individual photons.[1] Due to the two-photon absorption mechanism, relatively low energy photons delivered in a short pulse could produce an effect equivalent to the absorption of a single, more energetic photon. The practical significance of the two-photon excitation mechanism was not realized until ultrashort pulse lasers were available.[2-4]

Relevance of multiphoton absorption for damage mechanisms involved in ultrashort pulse laser tissue interactions

In previous work on the interaction of pulsed, infrared laser sources on retinal pigment epithelial (RPE) cells, we demonstrated that effects normally requiring visible or near UV (UVA) light exposure, such as excitation of melanin fluorescence[5] and DNA breakage,[6,7] could be produced by ultrashort infrared (810 nm) laser pulses. It was proposed that these effects were due to multiphoton absorption within the melanin of the RPE cells. Other authors have also reported two-photon excitation of melanin fluorescence.[8,9] Two-photon excitation effectively upconverted the infrared photons to UVA-VIS wavelengths, which then activated mechanisms that induced single and double strand DNA breaks.[7,10] Although an increased number of DNA strand breaks were demonstrated at threshold radiant exposures, the differences observed between the effects of continuous wave exposures, which would not be expected to induce multiphoton effects, and ultrashort pulse exposures, which might produce bioeffects due to multiphoton absorption, have been difficult to document consistently. In this report, we present our experimental data on the ability of ultrashort laser pulses to break genomic DNA, as well as a theoretical prediction of the number of photons likely to be absorbed in cellular targets during

short laser pulses. This analysis indicates that multiphoton absorption in the RPE melanosome is not likely to contribute to threshold damage, although it probably contributes to suprathreshold cellular damage due to induction of photo-oxidative stress, for example, as shown by Denton et al.[11]

METHODS

The hTERT-RPE cell line and comet assay for DNA breakage

Experiments were performed on a line of human-derived RPE cells provided by the Geron Corp. (Menlo Park, CA). These cells, designated hTERT-RPE, have been transfected with the gene for human telomerase (hTERT) and do not become senescent in culture; however, in other respects the cells exhibit a normal phenotype.[12,13] The hTERT-RPE cells produce melanin pigmentation in culture,[14] and most of the cells used in these experiments exhibited a degree of pigmentation proportional to their time in culture. The hTERT-RPE cells were grown for at least 2 weeks in 24-well, plastic culture plates, in standard Dulbecco's Modified Eagle's Medium (DMEM) containing 10% serum. During the laser exposures, the overlying media was drained from the wells and replaced with Dulbecco's Phosphate Buffered Saline (DBPS). Further details of the procedures for handling the hTERT-RPE cells were described elsewhere.[7]

Assessment of DNA breakage by comet assay

The use of the comet assay for detecting DNA strand breaks in RPE cells was reported by Hall et al.[6] Following electrophoresis of the lysed RPE cells in agarose gels, DNA fragments were stained with Syber Yellow, a fluorescent nucleic acid stain (Molecular Probes, Eugene, OR). The fluorescent DNA patterns (comets) were imaged with a fluorescence microscope equipped with a CCD imaging system (Optronics DEI-470), and the images processed with a public domain, comet assay analysis macro for the NIH/Scion-Image software[15], in order to extract comet tail length, tail moment (product of length and intensity), and comet area. Statistical analysis of the results was done using the Bonferroni multiple comparison test in the ProStat statistical package (Poly Software International, Pearl River, NY).

A modification was made to the analysis algorithm to address the problem that high-intensity fluorescent figures, such as those from control samples, were scored by the algorithm as having

very large comet tail lengths and moments. The algorithm used in our earlier experiments[7] sometimes reported larger comet tails and moments for the cells in the control conditions than for cells in the experimental conditions, although by eye, the control comets appeared to be "rounder" and less comet-like. The original comet analysis algorithm[15] operated by thresholding the comet image, then measuring the length and width of the border of the threshold image. We originally used the same absolute threshold for all comets in a given experiment, to avoid using a subjective setting for the analysis. This introduced an artifact, however, by over-emphasizing the size of bright comets, when the threshold was set to detect the outline of less intense comets. This was due to the fact that the comets in the control conditions tended to be very intense (the DNA did not migrate in the gel, but remained near the location of the cell nucleus), while the comets in experimental conditions tended to be relatively less intense (the DNA with an increased number of breaks migrated through the gel during electrophoresis, and therefore was more dilute). To minimize this problem, the analysis algorithm was modified so that the threshold for a given comet was set to 65% of the maximum white level of that particular image. In effect, the threshold used to determine the comet length was determined by a fixed ratio based on the dynamic range of the comet image, not at an absolute level. The 65% level was derived empirically, i.e. it was the threshold setting that did not over-emphasize the size of the control comets, while still detecting the comet tails in the experimental conditions. This modification was justified because the absolute white level and contrast range varied among different cell samples.

Melanosome preparation and hTERT-RPE cell melanosome loading

RPE cells were isolated from bovine eyes purchased from AnTech (Tyler, TX). Following sonication to release the cells' contents, the melanosomes were isolated by successive centrifugation using methods previously reported.[16] The melanosomes were stored frozen in 0.25 M sucrose at -20° C until use. The stock melanosome suspension contained approximately 6×10^9 (±20%) granules/ml, as determined by haemocytometer counts. Melanosomes were layered onto confluent cultures of hTERT-RPE 24 h prior to laser exposures, following the method of Denton et al.[11] Excess melanosomes were removed prior to laser exposure by rinsing the cells in normal DMEM.

Laser sources and exposures

The laser source used in the hTERT-RPE cell exposure experiments was a Coherent (Santa Clara, CA) MIRA 900F Ti:Sapphire regenerative amplifier system, modified from the system originally described by Noojin et al.[17] This system could be operated to produce either CW output at 810 nm, or mode-locked pulses. In mode-locked (ML) operation, it was anticipated that the laser produced an 80 MHz output train of ~48-fsec pulses with a 40 nm bandwidth centered at 810 nm. Subsequent beam analysis, however, revealed that the pulse widths produced were actually between 200 and 300 fsec. This discrepancy may have played a critical role in the determination of the threshold damage mechanisms, as will be discussed later in this section.

An external lens was used to focus the 810 nm beam onto the sample plane. The beam diameter at 1/e was 0.210 mm at the RPE cell monolayer on the culture plate. The laser was delivered to the cells in an exposure of 0.25 s duration, and the average power of both the CW and the train of mode-locked, ultrashort pulses was set to either 80 or 160 W/cm^2 depending on the experiment. These values were estimated as the irradiance equivalent to the corneal irradiance corresponding to 0.5 x ED_{50} and 1 x ED_{50}, respectively, for a retinal lesion in the intact (human) eye. The average power of both laser sources was measured with a Molectron (Portland, OR) EPM 1000 meter equipped with a PowerMax PM-10 thermopile detector. Just prior to the onset of the laser exposures, the culture well was drained of excess culture medium, and replaced with 100 µl of DPBS. To expose as many cells in each culture well as possible, the laser was scanned over the well, delivering the 0.25 s exposures in a spiral pattern. Approximately 1,261 exposures were required to expose each well.

The cells were exposed to the 810 nm CW and ML laser as follows: (1) controls received no laser exposure, but were handled in a similar fashion to the laser-exposed cells; (2) exposed to the 810 nm ML pulses at the estimated ED_{50} exposure required to produce a retinal lesion (~160 W/cm^2) (note: the pulses were originally thought to be 48-fsec pulsewidth, but were actually ~250-fs at 80 MHz in a train of 0.25 sec duration), (3) exposed to the 810 nm ML pulses at 0.5 x ED_{50} (~80 W/cm^2), (4) exposed to 810 nm laser in CW mode at the ED_{50} (0.25 sec at 160 W/cm^2), or (5) exposed to 810 nm CW mode laser at 0.5 x ED_{50} (0.25 sec at 80 W/cm^2).

RESULTS

Evidence for multiphoton absorption in the RPE cells

Evidence for multiphoton absorption produced by the ultrashort pulse laser exposures was provided by the observation of melanin fluorescence excited by 810-nm ML pulses in melanosomes isolated from RPE cells.[5] The fluorescence observed in these experiments exhibited a similar wavelength maximum at approximately 525 nm as that elicited by single-photon excitation with the 406 nm output of a Kr-ion CW laser. The power dependence of the two-photon excited fluorescence, however, closely followed a second order function, as opposed to single-photon excited fluorescence, which was linearly dependent on the excitation power (Figure 1). This observation was consistent with two-photon excitation of melanin fluorescence by the ultrashort pulse, 810 nm laser.

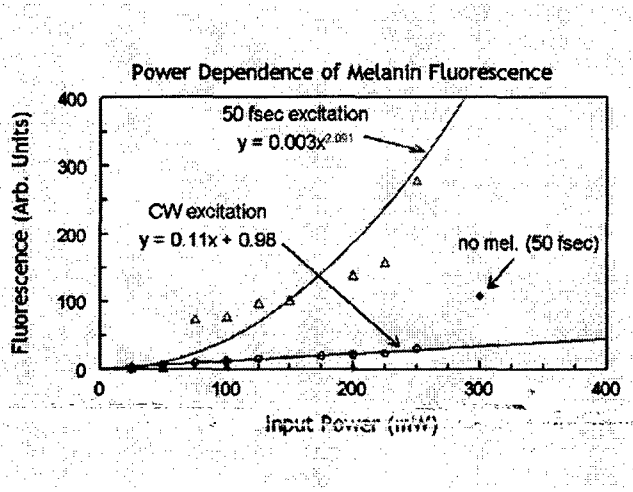

Figure 1: Power dependence of fluorescence in isolated RPE melanosomes

DNA damage by ultrashort and CW infrared laser exposure

These experiments compared the amount of DNA damage produced in cultured hTERT-RPE cells by exposures to 810 nm CW emissions and to ultrashort mode-locked (ML) laser pulses delivering equivalent average power to the cells. Two exposure conditions were examined: one-half the ED_{50} fluence required for retinal lesion threshold (80 W/cm^2), and threshold (ED_{50}) fluence (160 W/cm^2). The experiments were conducted with hERT-RPE cells not supplemented

with melanosomes. These cells spontaneously produce melanin pigment in their cytoplasm,[14] but were only lightly pigmented at the time these experiments were carried out. The effects of the laser exposures on the cells were assessed by determining single and double DNA strand breaks released by alkaline hydrolysis of the cells, using the comet assay procedure described above ("Assessment of DNA breakage by comet assay"). The results of the 0.5 x ED_{50} exposures are shown in Figure 2A, and the results of the ED_{50} exposures are shown in Figure 2B. At 0.5 x ED_{50}, cells exposed to ML laser pulses had slightly longer comet tail lengths than did the CW-exposed cells (Figure 2A). The difference was significant ($p<.001$, Bonferroni multiple comparison test). The comet tail lengths of the CW-exposed cells were not significantly different from those of the control cells. At the ED_{50} (Figure 2B), the comet tail lengths in both the CW and ML groups were significantly longer than in the control cells ($p<.005$), and the tail lengths of the ML-exposed cells were longer than those of the CW-exposed cells ($p<.02$), suggesting that the ML pulses were more effective in producing DNA strand breaks. The data, however, were somewhat inconsistent, because the comet tail moments, a measure of the density of the DNA in the "tails", were not significantly different among any of the exposure groups. The conclusion, that ML pulses were inducing multiphoton absorption effects in the RPE cells, was rendered less compelling by the inconsistency of the comet assay results.

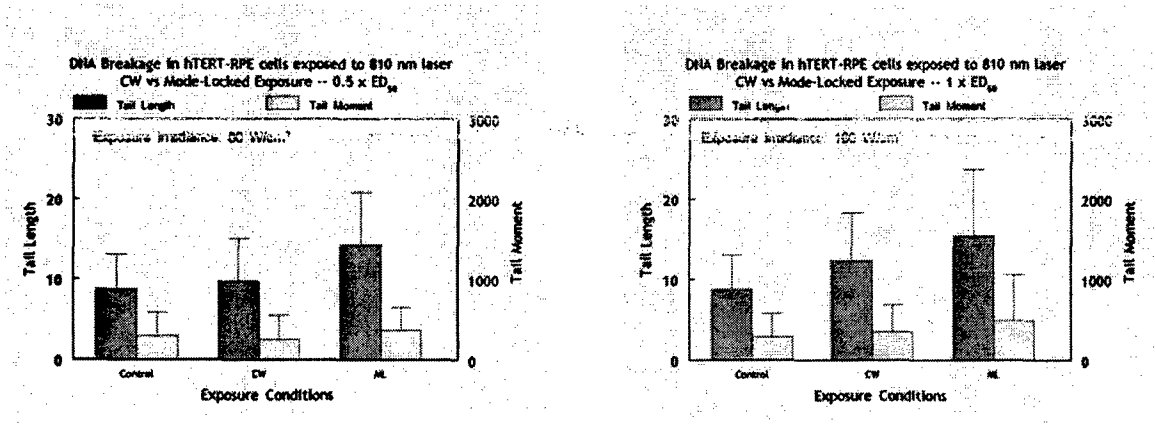

Figure 2: Comet assays of unpigmented hTERT-RPE cells exposed to CW and ML 810-nm laser. Figure 2A (left) shows results from exposures at 80 W/cm^2 (0.5 x ED_{50}). Figure 2B (right) shows results from exposures at 160 W/cm^2 (1 x ED_{50}).

DNA damage as a function of pigmentation load

Previous work in this laboratory,[16,18] as well as by that of Denton et al.,[11] indicated that the presence of melanin pigmentation could increase the susceptibility of RPE cells to photo-oxidative stress. Based on these observations, experiments were performed to measure DNA damage in cells with artificially enhanced pigmentation. RPE cell cultures with different pigmentation loads were produced by the melanosome supplementation protocol described above, and then exposed at the ED_{50} fluence (160 W/cm^2) to the CW and ML laser protocols.

Under these conditions, only cells with the highest levels of melanin pigmentation, i.e. the cells supplemented with 60 or 180 μl of melanosomes, had significantly greater DNA damage as assessed by comet tail length and moment ($p<.03$, Bonferroni multiple comparison test). These data are shown in Figure 3. Interestingly, in the heavily pigmented cells suffering the most DNA strand breaks, there was no significant difference between the comet assays in the CW and ML exposed cells. This finding indicated that multiphoton absorption was not involved – or at least not exclusively involved – in the production of the DNA strand breaks under these laser exposure conditions. These results must be qualified, however, due to the recent discovery that the duration of the ML pulses was in fact approximately 250 fs. Multiphoton absorption obviously becomes less likely for a given irradiance as the pulse width increases and the photon density decreases.

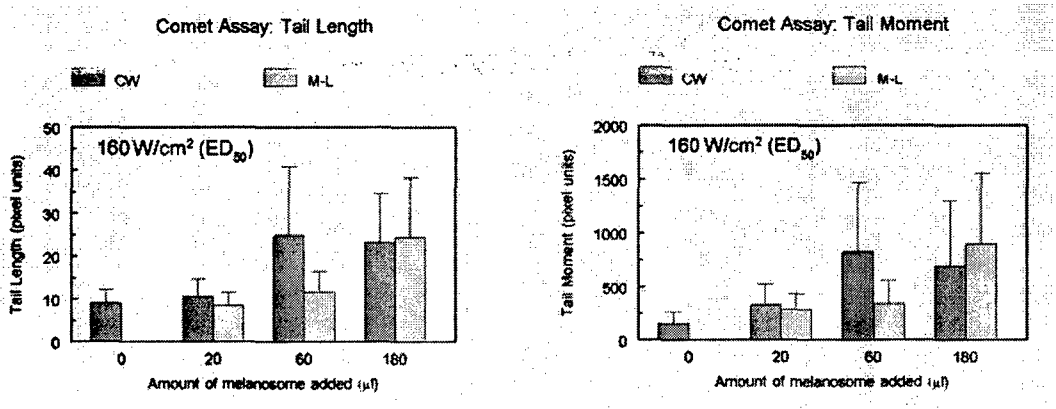

Figure 3: Comet assay results with HTERT-RPE cells pigmented by melanosome supplementation. All exposures were made at the ED_{50} (160 W/cm^2). Figure 3A (left): comet tail length measurements. Figure 3B (right): comet tail moment measurements.

In order to emphasize the effect of cellular pigmentation load, the results from the melanosome-supplemention experiment were replotted in Figure 4. Restricting the comet assay analysis to tail length, the amount of DNA breakage, as a function of the amount of isolated melanosomes added to the cells, is shown in Figure 4. Our previous work clearly showed that cellular pigmentation is directly related to the amount of melanosome supplementation, cf. Figure 2 in Glickman et al., 2003[7]. The trend of the data in Figure 4 indicates that there was little or no increase in DNA damage until at least 60 μl of melanosomes were added to the cells. While the difference in cellular pigmentation was a major determinant in the extent of DNA strand breakage, the laser output mode, i.e. CW or ML, appeared to be less important. This observation motivated us to calculate the number of photons absorbed in a typical RPE cell melanosome during the laser exposures used in these experiments, and, to determine if sufficient photons were being absorbed to make multiphoton absorption a likely (or even possible) outcome. These calculations are developed in the following sections.

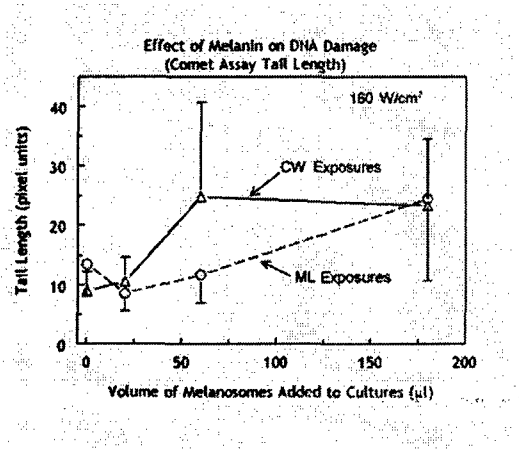

Figure 4: DNA strand breakage following CW or ML laser, as a function of the amount of cellular melanin pigmentation. Exposures were made at the ED_{50} (160 W/cm^2).

Photon energy available for absorption in melanin

Initially, the energy available in each photon is calculated:[19]

$$E = h\frac{c}{\lambda} \qquad (1)$$

This calculation yields 2.44×10^{-19} J as the energy of each 810 nm photon. Next, the number of photons available in a single laser pulse is calculated for the case of a 160 W/cm^2 laser and a 250 fs pulse duration (this was the actual pulsewidth used in the experiments; the planned pulsewidth

of 48 fs was not available). The total energy per pulse is thus 4×10^{-11} Joules/cm^2. The number of 810 nm photons available per square centimeter is then 1.6×10^8.

The time for electron de-excitation is assumed to be less than 1×10^{-8} seconds (80 MHz pulse repetition rate), so that the energy from each pulse is assumed to be non-additive. Another simplifying assumption is that only the physical area of a melanin granule is available for interaction with the photons. A melanin granule roughly approximates a rod, 5 microns in length with a 1 micron diameter,[20,21] so the maximum surface area presenting for interaction would be approximately a rectangular area of 5 square microns (1 micron × 5 microns or 5×10^{-8} cm^2). Thus, the maximum number of photons available for primary interaction with a melanin granule would be

$$5 \times 10^{-8}\,\text{cm}^2 \times 1.6 \times 10^8 \text{ photons/cm}^2 = 8 \text{ photons} \qquad (2)$$

This does not account for the cylindrical nature of the granule, assumes all photons intersect the granule along the long axis, and should lead to an overestimate of the number of interacting photons, if area of the granule is the primary parameter for absorption. Reducing the pulse irradiance from 160 W/cm^2 or reducing the width of the pulse will only reduce the number of photons available to interact with the granule. A minimum of approximately 200 W/cm^2 would be needed at 48 fs to result in 2 photons intersecting a single granule.

Extrapolating to the near infrared from the visible spectrum absorption coefficient (μ_a) of melanin reported by Sardar et al.[22] yields a value of 0.55 cm^{-1} for μ_a of melanin at 810 nm. If a simplifying assumption is made that the average thickness of the cylinder is 0.5×10^{-4} cm, then using Beer's law, the number of photons penetrating the granule would be

$$8\left(e^{-0.55\,\text{cm}^{-1} \times 0.5 \times 10^{-4}}\right) = 7.99978 \qquad (3)$$

This would result in 2.2×10^{-4} primary photons (i.e. 8.0 incident photons minus 7.99978 exiting photons) absorbed per granule. This does not account for potential attenuation of photons in materials that might result in some energy transfer to the granules.

Photons required to cause breaks

Note that the wavelength for maximum biological effect of DNA in cells is 270 nm, and 3 × 270 = 810 nm, implying that three photons could possibly be effective at causing DNA damage. Assuming that the weak hydrogen bonds associated with DNA require approximately 3 eV to break, and the energy of each 810 nm photon is

$$E = 2.44\times10^{-19}\ \frac{\text{J}}{\text{photon}} \cdot \frac{1\,\text{eV}}{1.6\times10^{-19}\,\text{J}} = 1.525\ \text{eV per photon.} \qquad (4)$$

In this case, a minimum of 2 photons would be required to cause a break. If there is 100% absorption in each granule, and it is assumed to be absorbed on the side (rather than on end), then 8 photons would be available to produce ionization. Scaling this, only 40 W would be needed at 100% absorption to achieve a break. More realistically, if the absorption coefficient for melanin were used in the calculation, then the minimum energy required for the actual absorption of two photons with total transfer of their energy to the melanosome (using previous simplifying assumptions regarding area and thickness) would be predicted as:

$$\frac{160\ \text{W}}{2.2\times10^{-4}\ \text{photons absorbed}} \cdot \frac{2\ \text{photons}}{5\times10^{-8}\,\text{cm}^2} = 2.9 \times 10^{13}\ \text{W/cm}^2 \qquad (5)$$

This calculation assumes that the NIR absorption coefficient for melanin given above, 0.55 cm^{-1}, applies, and only primary photons are present.

Range of laser exposures predicted to involve multiphoton absorption as a major damage mechanism

The number of photons expected to impact a melanosome as a function of laser radiant exposure can be predicted using the methodology described in the previous sections. Some representative calculations have been done for a physiologically relevant range of exposures, and are presented

graphically below in Figures 5 and 6. Note that these graphs indicate only the number of photons incident on a typical, 1 x 5 μm, RPE melanosome, not the number of photons actually (or realistically) absorbed in the pigment granule.

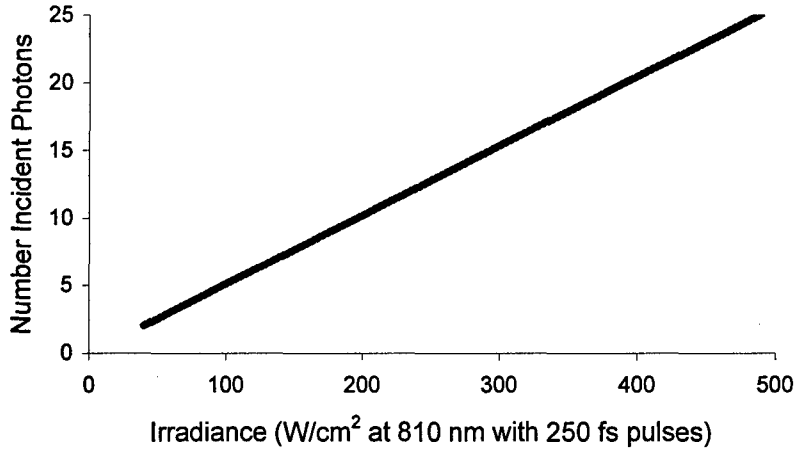

Figure 5: Number of photons incident on a RPE melanosome as a function of irradiance

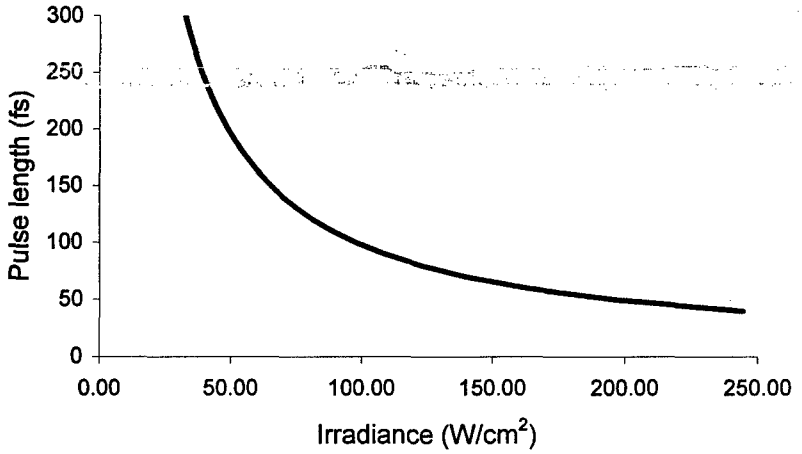

Figure 6: Pulse duration required to produce sufficient irradiance for at least two 810-nm photons to be incident upon a RPE melanosome.

DISCUSSION

Implication of results

Recent investigation of the principal damage mechanisms induced in ocular tissue by ultrashort pulse (<100 fs) lasers, have shown that laser-induced breakdown has the lowest energy threshold, and therefore is probably the predominant damage mechanism at fluences near the ED_{50} for retinal and RPE lesions.[17,23,24] At suprathreshold fluence, other mechanisms are activated, including photochemical reactions producing oxidative endpoints.[25,26] After our initial observation of increased DNA strand breaks following exposure of cultured RPE cells to ultrashort pulse laser, compared to CW exposures delivering the equivalent average power,[6] we proposed that a damage mechanism activated by multiphoton absorption was responsible for the difference. We reported that two-photon excitation of fluorescence in isolated RPE melanosomes was due to multiphoton absorption, but the fluorescence was observed at suprathreshold irradiance.[5] The present investigation of DNA strand breaks in RPE cells at subthreshold and threshold irradiance indicated that cellular melanin plays a role in mediating the DNA damage, but it was not clear that multiphoton absorption was responsible for the damage near the presumptive threshold fluence. This conclusion was primarily based on the finding of similar amounts of DNA damage produced by both CW and ML laser exposures at threshold irradiance. The theoretical analysis developed in this paper also supported the conclusion that, at threshold, an insufficient number of photons are absorbed in a RPE melanosome to result in multiphoton absorption.

Some qualifications must be considered in reaching this conclusion. In the analysis reported here, only primary photons, that is, photons that travel directly from the source to the target are considered. Scattered photons are not included, but are not expected to contribute significantly to the multi-photon effect. Another consideration is that there may be a specific "resonance" effect that causes a significant change in the absorption properties of a melanin granule that has yet to be described. For that matter, the optical properties of RPE melanin in the near infrared optical radiation band have not been precisely measured. The values used in our analysis represent a reasonable extrapolation from the optical properties of melanin measured in the visible spectrum. Additionally, the area of interaction is assumed to be at the most favorable presentation for absorption, and the cylindrical nature of the granule is not included, so the physical interaction

area used in these calculations is greater than the actual physical size of the granule. Physical size is not always directly proportional to absorption coefficients, and it is known that resonance reactions exist for many photon interactions.[19]

Other mechanisms besides direct photon absorption may also play an important role in determining the damage to melanin granules. If melanin has undiscovered or unusual properties, such as the ability to exist as a stable free radical,[27] then the melanosome may be able to maintain electrons in an excited state such that high repetition rate photon pulses can produce additive (pulse to pulse) effects. In such a case, multiphoton effects would then be possible at lower peak power exposures than indicated by our analysis. In the absence of such properties, however, individual pulses would require supra-threshold energies on the order of megawatts to initiate multi-photon effects by primary photons.

Contribution of non-linear interactions to possible multiphoton effects

Any of the non-linear interactions known to occur with ultrashort laser pulses[28-30] could possibly cause multiphoton interactions to occur. The photon concentrations produced could be sufficient to cause localized ionization in each case. The concentration of photons would be altered by the non-linear reaction, for example through the effects of self-focusing, which might result in sufficient energy deposition leading to alteration of absorption coefficients with resulting concentration of energy. Such phenomena could manifest themselves as plasma formation, thermal denaturation (probably highly localized), and/or oxidative damage.

Is multiphoton absorption mediated by other possible cellular targets?

Finally, the possibility exists that other intracellular targets may be involved in the interaction of ultrashort, infrared laser pulses. In the case of the RPE cell, we have concentrated on the melansome because of its prominent cytoplasmic location, its broadband optical absorption characteristics,[31] and its known involvement in ocular light[32] and laser[33] damage. The RPE melanin is clearly an important factor in mediating CW and ultrashort pulse damage, as indicated by the present results, and it appears to mediate photo-oxidative stress produced by suprathreshold, ultrashort pulse exposures.[26] Nevertheless, at threshold, other cellular structures may play a role in cellular responses to ultrashort laser pulses. Mitochondria are possible targets, but – as is also the case with the melanosomes - it is unclear how, in the short term, damage to

these cytoplasmic organelles could affect the nuclear DNA. Potential targets for laser damage exist in the nucleus. As noted above, the absorption maximum for DNA damage occurs near 270 nm; therefore, a suitable absorber to mediate multiphoton absorption of near infrared photons has to be identified. The genomic DNA in eukaryotic cells itself exists in nucleosomes, repeating complexes of DNA and histone proteins. The diameter of these structures is on the order of 30 nm,[34] which is a much smaller cross-section compared to the RPE melanosomes, and presumably would absorb incident NIR photons at much lower efficiency. The chain of nucleosomes comprising the DNA, however, forms an assemblage that is much larger than the individual subunits, and if the entire complex functioned as a single, absorbing unit, then the effective absorption cross-section would be correspondingly larger. Whether the entire nuclear DNA-histone complex functions as a single absorber to promote multiphoton absorption at suprathreshold laser exposures remains to be determined. In addition, better measurements of the near infrared optical properties of cellular organelles are required in order to evaluate hypothetical non-linear laser bioeffects.

REFERENCES FOR SECTION ONE

1. M. Goppert-Mayer, "Über Elementarakte mit zwei Quantensprüngen", *Annalen der Physik* **9**, pp. 273-294, 1931.
2. W. Denk, J. H. Strickler, and W. W. Webb, "Two-photon laser scanning fluorescence microscopy", *Science* **248**, pp. 73-76, 1990.
3. K. Konig, P. T. So, W. W. Mantulin, B. J. Tromberg, and E. Gratton, "Two-photon excited lifetime imaging of autofluorescence in cells during UVA and NIR photostress", *J. Micros.* **183**, pp. 197-204, 1996.
4. K. Konig, Y. Liu, G. J. Sonek, M. W. Berns, and B. J. Tromberg, "Autofluorescence spectroscopy of optically trapped cells", *Photochem. Photobiol.* **62**, pp. 830-835, 1995.
5. R. D. Glickman, B. A. Rockwell, G. D. Noojin, D. J. Stolarski, and M. L. Denton, "Evidence for excitation of fluorescence in RPE melanin by multiphoton absorption". In *Laser-Tissue Interaction XIII:Photochemical, Photothermal, and Photomechanical,* (Edited by S. L. Jacques, D. D. Duncan, S. J. Kirkpatrick, and A. Kriete), Proc. SPIE Vol. **4617**, pp. 172-179, SPIE, Bellingham, WA, 2002.

6. R. M. Hall, R. D. Glickman, B. A. Rockwell, N. Kumar, and G. D. Noojin, "Pulsewidth-dependent nature of laser-induced DNA damage in RPE cells". In *Laser-Tissue Interaction: Photochemical, Photothermal, and Photomechanical*, (Edited by D. D. Duncan, S. L. Jacques, and P. C. Johnson), Proc. SPIE Vol. **4257**, pp. 159-166, SPIE, Bellingham, WA, 2001.
7. R. D. Glickman, N. Kumar, B. A. Rockwell, G. D. Noojin, M. L. Denton, and D. J. Stolarski, "Melanin and the cellular effects of ultrashort pulse, near infrared laser radiation". In *Laser-Tissue Interaction XIV*, (Edited by S. L. Jacques, D. D. Duncan, S. J. Kirkpatrick, and A. Kriete), Proc. SPIE Vol. **4961**, pp. 97-105, SPIE, Bellingham, WA, 2003.
8. K. Hoffmann, M. Stucker, P. Altmeyer, K. Teuchner, and D. Leupold, "Selective femtosecond pulse-excitation of melanin fluorescence in tissue", *J. Invest. Dermatol.* **116**, pp. 629-630, 2001.
9. K. Teuchner, W. Freyer, D. Leupold, A. Volkmer, D. J. Birch, P. Altmeyer, M. Stucker, and K. Hoffmann, "Femtosecond two-photon excited fluorescence of melanin", *Photochem. Photobiol.* **70**, pp. 146-151, 1999.
10. R. D. Glickman, "Phototoxicity to the retina: Mechanisms of damage", *International Journal of Toxicology* **21**, pp. 473-490, 2002.
11. M. L. Denton, D. M. Eikum, G. D. Noojin, D. J. Stolarski, R. J. Thomas, R. D. Glickman, and B. A. Rockwell, "Pigmentation in NIR laser tissue damage". In *Laser and Noncoherent Light Ocular Effects: Epidemiology, Prevention, and Treatment*, (Edited by B. E. Stuck and M. Belkin), Proc. SPIE Vol. **4953**, pp. 78-84, SPIE, Bellingham, WA, 2003.
12. X. R. Jiang, G. Jimenez, E. Chang, M. Frolkis, B. Kusler, M. Sage, M. Beeche, A. G. Bodnar, G. M. Wahl, T. D. Tlsty, and C. P. Chiu, "Telomerase expression in human somatic cells does not induce changes associated with a transformed phenotype", *Nature Genetics* **21**, pp. 111-114, 1999.
13. A. G. Bodnar, M. Ouellette, M. Frolkis, S. E. Holt, C. P. Chiu, G. B. Morin, C. B. Harley, J. W. Shay, S. Lichtsteiner, and W. E. Wright, "Extension of life-span by introduction of telomerase into normal human cells. [see comments.]", *Science* **279**, pp. 349-352, 1998.
14. L. Rambhatla, C.-P. Chiu, R. D. Glickman, and C. Rowe-Rendleman, "In vitro differentiation capacity of telomerase immortalized human RPE cells", *Invest. Ophthalmol. Vis. Sci.* **43**, pp. 1622-1630, 2002.

15. C. Helma and M. Uhl, "A public domain image-analysis program for the single-cell gel-electrophoresis (comet) assay", *Mut. Res.* **466**, pp. 9-15, 2000.
16. A. E. Dontsov, R. D. Glickman, and M. A. Ostrovsky, "Retinal pigment epithelium pigment granules stimulate the photo-oxidation of unsaturated fatty acids", *Free Rad. Biol. Med.* **26**, pp. 1436-1446, 1999.
17. G. D. Noojin, C. P. Cain, C. A. Toth, D. J. Stolarski, and B. A. Rockwell, "Comparison of retinal damage thresholds of laser pulses in the macula/paramacula regions of the live eye". In *Laser-Tissue Interaction X: Photochemical, Photothermal, and Photomechanical*, (Edited by S. L. Jacques, G. J. Müller, A. Roggan, and D. H. Sliney), Proc. SPIE Vol. **3601**, pp. 39-42, SPIE, Bellingham, WA, 1999.
18. R. D. Glickman, M. Natarajan, N. Kumar, and F. Roldan, "Photo-oxidative stress produces a biphasic pattern of NF-κB activation in cultured retinal pigment epithelial cells", *Free Rad. Biol. Med.* **33**, p. S428, 2002.
19. H. Cember, *Introduction to Health Physics*, McGraw-Hill Professional, New York, 1996.
20. R. D. Glickman, J. M. Gallas, S. L. Jacques, B. A. Rockwell, and D. K. Sardar, "Physical and photochemical properties of ocular melanin". In *Saratov Fall Meeting 2000: Optical Technologies in Biophysics and Medicine II*, (Edited by V.V. Tuchin), Proc. SPIE Vol. **4241**, pp. 112-123, SPIE, Bellingham, WA, 2001.
21. R. D. Glickman, "The origin of photo-oxidative stress in the aging eye", *Progr.Brain Res.* **131**, pp. 699-712, 2001.
22. D. K. Sardar, M. L. Mayo, and R. D. Glickman, "Optical characterization of melanin", *J. Biomed. Opt.* **6**, pp. 404-411, 2001.
23. C. P. Cain, C. A. Toth, G. D. Noojin, V. Carothers, D. J. Stolarski, and B. A. Rockwell, "Thresholds for visible lesions in the primate eye produced by ultrashort near-infrared laser pulses", *Invest. Ophthalmol. Vis. Sci.* **40**, pp. 2343-2349, 1999.
24. R. J. Thomas, G. D. Noojin, P. K. Kennedy, B. A. Rockwell, K. S. Denning, J. Shaver, and G. D. Buffington, "Laser damage threshold trends for sub-100 fs pulses in the retina". In *Laser-Tissue Interaction XIII: Photochemical, Photothermal, and Photomechanical*, (Edited by S. L. Jacques, D. D. Duncan, S. J. Kirkpatrick, and A. Kriete), Proc. SPIE Vol. **4617**, pp. 141-149, SPIE, Bellingham, WA, 2002.

25. M. L. Denton, D. M. Eikum, D. J. Stolarski, G. D. Noojin, R. J. Thomas, R. D. Glickman, and B. A. Rockwell, "Hydrogen peroxide production in cultured RPE cells exposed to near infrared lasers". In *Laser Tissue Interaction XIII: Photochemical, Photothermal, and Photomechanical*, (Edited by S. L. Jacques, D. D. Duncan, S. J. Kirkpatrick, and A. Kriete), Proc. SPIE Vol. **4617**, pp. 150-155, SPIE, Bellingham, WA, 2002.

26. M. L. Denton, D. M. Eikum, D. J. Stolarski, G. D. Noojin, R. D. Thomas, R. D. Glickman, and B. A. Rockwell, "Cytotoxicity in cultured RPE: A comparative study between continuous wave and mode-locked lasers". In *Laser-Tissue Interaction XIII: Photochemical, Photothermal,, and Photomechanical*, (Edited by S. L. Jacques, D. D. Duncan, S. J. Kirkpatrick, and A. Kriete), Proc. SPIE Vol. **4617**, pp. 156-160, SPIE, Bellingham, WA, 2002.

27. P. A. Riley, "Radicals in melanin biochemistry", *Ann. NY Acad. Sci.* **551**, pp. 111-120, 1988.

28. P. K. Kennedy, S. A. Boppart, D. X. Hammer, B. A. Rockwell, G. D. Noojin, and W. P. Roach, "A first-order model for computation of laser-induced breakdown thresholds in ocular and aqueous media: Part II -- comparison to experiment", *IEEE J. Quantum. Electron.* **QE-31**, pp. 2250-2257, 1995.

29. C. P. Cain, C. D. DiCarlo, B. A. Rockwell, P. K. Kennedy, G. D. Noojin, D. J. Stolarski, D. X. Hammer, C. A. Toth, and W. P. Roach, "Retinal damage and laser-induced breakdown produced by ultrashort-pulse lasers", *Graefes Arch.Clin.Exper.Ophthalmol.* **234 Suppl 1**, pp. S28-S37, 1996.

30. B. A. Rockwell, D. X. Hammer, R. A. Hopkins, D. J. Payne, C. A. Toth, W. P. Roach, J. J. Druessel, P. K. Kennedy, R. E. Amnotte, B. Eilert, S. Phillips, G. D. Noojin, D. J. Stolarski, and C. Cain, "Ultrashort laser pulse bioeffects and safety", *J. Laser Appl.* **11**, pp. 42-44, 1999.

31. T. Sarna, "Properties and function of the ocular melanin - A photobiophysical view", *J. Photochem. Photobiol. B* **12**, pp. 215-258, 1992.

32. W. T. Ham Jr, R. G. Allen, L. Feeney-Burns, M. F. Marmor, L. M. Parver, P. H. Proctor, D. H. Sliney, and M. L. Wolbarsht, "The involvement of the retinal pigment epithelium (RPE)". In *Optical Radiation and Visual Health*, (Edited by M. Waxler and V. M. Hitchins), pp. 43-67, CRC Press, Boca Raton, FL, 1986.

33. C. R. Thompson, B. S. Gerstman, S. L. Jacques, and M. E. Rogers, "Melanin granule model for laser-induced thermal damage in the retina", *Bull. Math. Biol.* **58**, pp. 513-553, 1996.

34. S. H. Leuba, C. Bustamante, J. Zlatanova, and K. van Holde, "Contributions of linker histones and histone H3 to chromatin structure: Scanning force microscopy studies on trypsinized fibers", *Biophys. J.* **74**, pp. 2823-2829, 198.

SECTION TWO

Intracellular signaling mechanisms responsive to laser-induced photochemical and thermal stress

INTRODUCTION

The pigmented cells of the retinal pigment epithelium (RPE), by virtue of their melanin content, absorb light over a wide wavelength range. With sufficient irradiance, a variety of physiological and physical responses including disruption, denaturation, and photochemical damage may occur.[1-6] The particular form of the laser-induced damage is determined by the total energy delivered to the tissue, the rate of energy delivery, the wavelength of the irradiating light, and the optical properties of the irradiated tissue. While the response of tissue (especially ocular tissue) to laser exposure has been well studied at the morphological level, the understanding of the cellular response at the molecular level is still evolving. For example, it is becoming clear that oxidative stress may contribute to overall tissue damage, even if the laser exposure parameters primarily cause damage through thermal- or stress-confined conditions.[7-10] The present study was conducted to characterize the laser-induced response of intracellular signaling pathways that are known to be responsive to oxidative stress. One such signaling pathway is the transcription factor, NF-κB.[11]

The nuclear transcription factor, NF-κB, is a member of a set of proteins that controls the expression of several families of genes, especially "early" genes responding to stressors, as well as those involved in repair mechanisms.[12,13] The transcription factor itself is composed of subunits drawn from the "NF-κB" class, designated p50 and p52, as well as from the "Rel" class, including RelA (also known as p65), c-Rel, and RelB. These proteins share an N-terminal domain called the Rel homology (RH), that contains the regions subserving dimerization of the protein subunits, DNA binding, nuclear localization, and binding of an inhibitory subunit, IκB.[14] The most abundant form of the transcription factor in the cytoplasm of mammalian cells is a dimer consisting of a light component, p50, and a heavy component, the RelA, or p65, subunit. This dimer is commonly referred to by the generic name, NF-κB.[15] This dimer, when activated by release from its inhibitory subunit, IκB, is translocated into the nucleus, where it binds to genomic DNA κB binding sequences and initiates the expression of select genes (Figure 1). A

major hypothesis of the present work is that the melanin granules of the RPE cell represent potential centers for interaction with incident light or laser energy, and the absorption of this energy results directly in production of reactive species that produce oxidative damage to cellular sites. The activation of NF-κB appears to be a response to the laser-induced photo-oxidative stress.

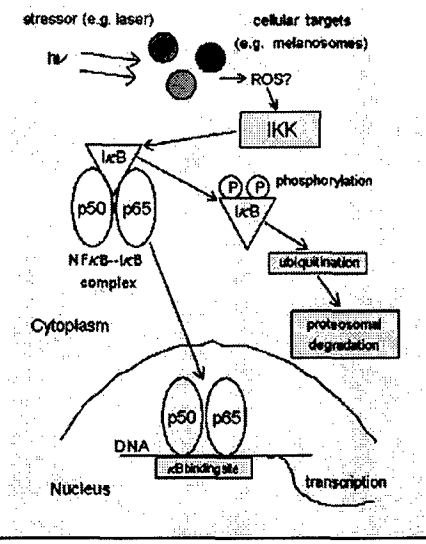

Figure 1. Schematic of NF-κB regulation, activation, degradation, and function. The figure illustrates the hypothetical activation and nuclear translocation of NF-κB following the absorption of incident light in the RPE melanosomes.

Regulation of NF-κB activity

The basic mechanism of regulation is that the NF-κB/Rel proteins are retained in the cytoplasm, bound to an inhibitory subunit, IκB, which blocks the nuclear localization sequence of the RH domain. This prevents the transcription factor from entering the nucleus until an appropriate external signal or stressor causes dissociation/degradation of IκB. IκB degradation is accomplished by phosphorylation of N-terminal serines in IκB by a specialized kinase, the IκB kinase complex (IKK). The second stage of inactivation involves ubiquitination of IκB lysine sites through an ATP-dependent reaction.[16,17] Once polyubiquitinated, IκB undergoes rapid degradation in the proteasome. Activation of the NF-κB subunits can occur rapidly, i.e., in minutes, after a sufficiently strong stimulus initiates the action of the IKK complex.[16] Two types of IKK (α and β) have been recognized with different and non-overlapping functions; however, this aspect will not be discussed further here. Following activation, the NF-κB is transported

into the nucleus by means of the nuclear localization sequence. Binding of the protein to κB sequences in the DNA cause transcription of large families of genes. Because there are actually several types of Rel/NF-κB protein subunits that can form homo- and heterodimers, and each dimer can bind to different κB sites in genome, a diversity of gene expression responses are possible, depending on the particular dimer activated.[18]

Stressors causing activation of NF-κB

Many external stressors activate NF-κB. There is a large literature describing NF-κB activation by toxins, pathogens (including bacteria and viruses), physiological stress (e.g. ischemia or shear stress), oxidative stress, and physical stress (e.g. hyperthermia), as reviewed by Pahl.[18] Other specific activators include inflammatory cytokines[19,20] and ionizing radiation.[21-23] With respect to the bioeffects of light, there has been much work on the effect of UV exposure and NF-κB activation in cells, which has found that the generation of reactive oxygen species is a critical precursor to activation of the transcription factor.[24-27] Moreover, UV exposure can activate NF-κB in enucleated cells, indicating that the sensitive receptor element mediating the activation is in the cytoplasmic compartment - most likely in the plasma membrane.[26,28] Changes in the oxidative (redox) state of the cell are tightly linked to the activity level of NF-κB.[29] Deliberate production of reactive oxygen species within the cell, for example in photodynamic therapy, is an effective activator of NF-κB.[30-32] Consistent with the role of oxidative stress as an activating agent, treatment with antioxidants usually reduces the activation of the transcription factor.[33-35]

Role of NF-κB activation

The genes activated by NF-κB are involved in a wide range of cellular activities and function. About 150 genes are known to be activated by NF-κB/Rel proteins.[18] These genes are involved in cellular repair, restoration and proliferation, as well as production of pro- and anti-apoptotic factors. Many of these genes have contrasting actions on the cell; not all the genes are activated by every NF-κB/Rel family member. Particularly noteworthy is that NF-κB activation is capable of modulating immune responses and mediating inflammatory reactions, as evidenced by its effect on the expression of pro-inflammatory cytokines, such as TNF-α and –β, IL-1α and –β, IL-6, and IFNα. Recognition of the role of NF-κB in promoting or mediating an inflammatory response after retinal laser injuries would be an important advance in understanding the cellular responses to - and possibly developing an effective therapy for - such

injuries. A central question is whether NF-κB activation represents a death (apoptotic) signal, or the initiation of a repair response. The answer to this question appears to be complex, and highly cell type-dependent. Depending on the cellular system, and the type of activating stress involved, NF-κB may either promote or prevent apoptosis.[36] In many pathological conditions, particularly in neurodegenerative conditions leading to accumulation of β-amyloid precursor in neurons, the activation of NF-κB prevents neuronal loss through apoptosis.[37] In contrast, NF-κB activated after ischemia or glutamate-induced neurotoxicity was found to be pro-apoptotic.[38, 39] In ocular light damage studies, after photo-oxidative stress, retinal photoreceptors that failed to activate NF-κB did not survive, undergoing cell death by either apoptosis or necrosis.[40, 41] Overall, it is probably more common for NF-κB to exert an anti-apoptotic action, i.e., the cellular genetic response initiated by NF-κB produces a reparative effect that prevents apoptosis, unless the external stressor exceeds the lethal threshold.[36] Regardless of the consequence of its activation, NF-kB serves as an indicator of oxidative stress. As noted above, its appearance in the nucleus (translocation) is a function of oxidative stress to the cell. There is an extensive literature on the effect of generalized UV exposure on NF-κB metabolism, e.g., see review by Legrand-Poels et al.[42] Characterization of NF-κB activation following laser injury to the retina and retinal pigment epithelium (RPE) may be a useful way to assess the severity of the laser injury, as well as the efficacy of experimental therapies. The research reported here has demonstrated that NF-κB is activated after sub-lethal laser exposure, and the degree of activation can be modulated by certain antioxidants, indicating that nuclear NF-κB levels are tied to the redox environment of the cell.

METHODS

In vitro cell model

These experiments were performed on hTERT-RPE cells, a line of human-derived retinal pigment epithelial (RPE) cells, stably transfected with the gene for human telomerase (the hTERT-RPE cell line was obtained from Geron Corporation, Menlo Park, CA). The presence of this gene prevents the onset of replicative senescence in these cells in culture; in other respects the cells exhibit a normal phenotype.[43,44] The cells were grown on plastic, 24-well culture plates, and were maintained at 37° C in Dulbecco's Minimum Essential Medium (DMEM) containing 10% calf serum under an atmosphere of 95% O_2 and 5% CO_2.

Laser irradiation

The hTERT-RPE cells were prepared for laser irradation by replacing the standard DMEM containing phenol red indicator with Dulbecco's Phosphate Buffered Saline (DPBS), which is colorless. The culture plates were placed on a computer-controlled X-Y stage, so that each well could be exposed to the laser for a set amount of time, or left unexposed as a control. Continuous wave (CW) exposures were made with a Coherent Model 920 Argon-ion laser, the output of which consisted of a mixture of the 488.1 nm line (55%) and the 514.5 nm line (45%). The culture plates were maintained at ambient room temperature during the exposure protocol. The exposure duration was 10 m at an irradiance of 0.5 W/cm^2. Laser power was measured with a Molectron PM3 thermopile detector driving an EP-1000 radiometer. This level of exposure has previously been demonstrated to produce markers of photochemcal stress in the cells, e.g. protein carbonyl adducts.[45] Following the laser exposure, the culture plates were returned to the 37° C incubator until the time points for harvesting the cells for analysis were reached.

NF-κB Assay

Cells were harvested at various time points up to 24 h post-exposure. They were freed from the culture plate at the desired time points by replacing the DPBS with 0.25% trypsin. After about 1 m, the cells were released and transferred into plastic microcentrifuge tubes. After washing twice with DPBS, the cells were pelleted and frozen at -70° C until analysis. For NF-κB analysis, nuclear extracts from the cells were subjected to an electrophoretic mobility shift assay (EMSA).[21] Briefly, the cells were thawed, resuspended in lysis buffer, and the nuclei were separated from the cytoplasmic lysate by centrifugation. Protein was extracted from the nuclei, loaded on polyacrylamide gels, and probed with ^{32}P-labeled, NF-κB-specific oligonucleotides. Binding to proteins in the gel was imaged by autoradiography. Quantification of the labeled bands in the gels was accomplished by densitometric analysis of the autoradiographic images using Image-Pro software (Media Cybernetics, Silver Spring, MD).

Antioxidant treatment of hTERT-RPE cells

Antioxidant treatment consisted of N-acetylcysteine (NAC) at 20 mM, ascorbic acid (AA, vitamin C) at 500 μM, or pyrrolidine dithiocarbamate (PDTC) at 100 μM. The antioxidant solutions were prepared in DPBS. Reagents were obtained from the Sigma Corporation (St. Louis, MO). The concentrations of the antioxidants were chosen based on previous experimental observations, e.g. with PDTC and NAC on human aortic endothelial cells[46], and with AA on bovine RPE cells.[47] The antioxidants in DPBS were tested individually, in different wells on a culture plate. The cells were incubated with the antioxidant for 30 m prior to laser exposure. Following this pretreatment, the cells were exposed to laser, and then prepared for NF-κB assay, as described above.

RESULTS

Induction of NF-κB by exposure of hTERT-RPE cells to CW visible laser

In non-irradiated hTERT-RPE cells, there was very little NF-κB (p50/p65 dimer) present (Figure 2A). The p50/p50 dimer was present, and was possibly constitutively expressed in these cells. In cells exposed to the CW argon-ion laser, the p50/p65 dimer rapidly appeared (Figure 2A). The specificity of the assay was evaluated by incubating the nuclear extracts with an excess of

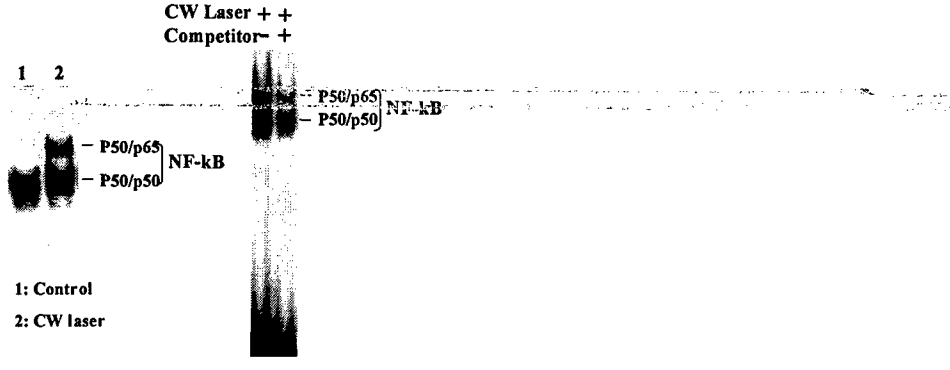

Figure 2. A (left): activation (nuclear translocation) of p50/p60 dimer in RPE cells exposed to laser (lane 2, 60 m post exposure assay), compared to unexposed controls (lane 1). The amount of p50/p50 dimer in the nucleus was not affected by laser exposure. **B** (right): Competitive experiment showing specificity of NF-κB DNA-binding activity in the EMSA assay. Nuclear extracts were incubated in the absence or presence of an excess of unlabelled NF-κB-binding oligonucleotide for 5 m, and then probed with ^{32}P-labelled probe. Competition by the unlabeled probe indicates specificity of assay.

unlabeled, homologous oligonucleotide competitor for 5 m, running the extracts on electrophoretic gels, and then probing the gels with ^{32}P-labeled NF-κB-specific oligonucleotides. The presence of the homologous competitor reduced the binding of the labelled, oligonucleotide probe (Figure 2B), demonstrating the specificity of the assay.

Time-course of NF-κB activation following CW laser exposure

CW argon-ion laser exposure of hTERT-RPE cells induced a biphasic pattern of NF-κB activation. After exposure to the mixed, 488 and 514 nm output of a CW Argon-ion laser for 10 m at an irradiance of 0.5 W/cm^2, an increase in nuclear NF-κB was detected as early as 1 h post-exposure, compared to unexposed cells, which exhibited little or no NF-κB activation. The activation followed a biphasic pattern, with a decline following the initial increase, followed by a second, higher increase by 24 h post-exposure (Figure 3). The early increase was likely due to activation of a pre-existing pool of cytoplasmic NF-κB (i.e., released from IκB), while the later increase probably represented *de novo* synthesis. Interestingly, this biphasic pattern was similar to that observed after exposure to ionizing radiation,[21] and was also reported after some types of photosensitized cell damage, with the delayed response component beginning at about 2 h post-treatment and continuing for 24 h.[42]

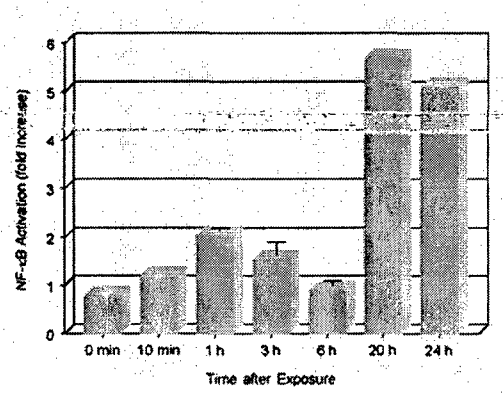

Figure 3. Biphasic activation of NF-κB DNA binding activity indicated by EMSA. RPE cells were harvested at the indicated times after the laser exposure protocol described in the text, and nuclear extracts were assayed for NF-κB. The amount of NF-κB found at each time point is indicated on the graph as a fold-increase over control. Error bars indicate the data range for 2 experiments.

Effects of antioxidant pretreatment on laser activation of NF-κB

Many reports, based on studies in diverse cell lines and utilizing a range of external stressors, indicate that the level of activation of NF-κB is modified by antioxidant treatment.[48] Two thiol-based antioxidants frequently reported to reduce the level of activated NF-κB are N-acetylcysteine (NAC) and pyrrolidine dithiocarbamate (PDTC). The ability of these agents to inhibit NF-κB nuclear translocation following laser exposure was tested in the hTERT-RPE cell line.

PDTC was tested at a concentration of 100 μM. The hTERT-RPE cells were incubated at 37° C for 30 m in DPBS containing 100 μM PDTC, and then exposed to CW argon-ion laser as described above. Cells were harvested for NF-κB assay at 1 h and 24 h post laser exposure. Pretreatment with PDTC failed to reduce the activation of NF-κB; indeed, the level of the factor in nuclear extracts was increased after PDTC, even in the absence of laser exposure (Figure 4).

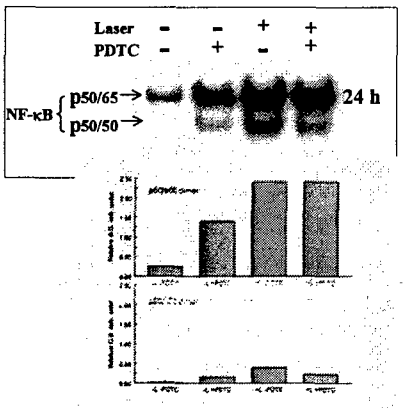

Figure 4. PDTC pretreatment of RPE cells does not reduce NF-κB activation by laser. RPE cells were incubated in 100 μM PDTC prior to laser exposure. NF-κB was assayed at 24 h and no change was found in the amount of p50/p65 dimer activated by the laser, compared to untreated cells. In addition, unexposed cells treated with PDTC exhibited higher levels of nuclear p50/p65 dimer. The amount of p50/p50 dimer in laser-exposed cells was slightly reduced by the PDTC treatment. Results of densitometric scans are shown below each lane in the EMSA assay gel. Upper bars: p50/p65; lower bars: p50/p50.

Similarly, pretreatment of the hTERT-RPE cells with NAC (20 mM in DPBS) did not reduce the laser-induced activation of NF-κB. At the 1 h and the 24 h assay time points, the laser-exposed cells treated with NAC had higher levels of nuclear NF-κB, compared to the untreated cells (Figure 5). Thus, the two thiol-based antioxidants did not reduce the stimulatory effect of the laser on the NF-κB signaling pathway, and possibly enhanced it.

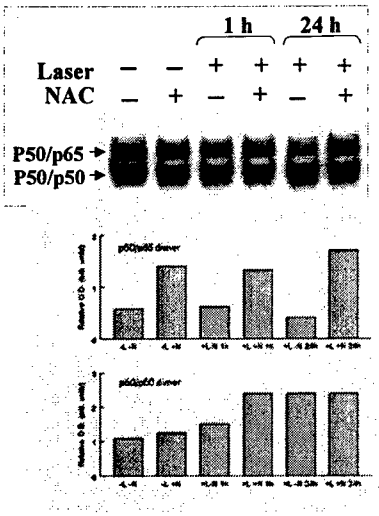

Figure 5. NAC pretreatment of RPE cells does not reduce NF-κB activation by laser. RPE cells were incubated in 20 mM NAC prior to laser exposure. This pretreatment did not reduce NF-κB activation either at 1 h or at 24 hr. In the absence of laser exposure, the NAC treatment increased the amount of NF-κB in the nuclear extracts. Results of densitometric scans are shown below each lane in the EMSA gel (upper bars:

In contrast to the two thiol-based antioxidants, the 30 m pretreatment of the hTERT-RPE cells with AA (500 μM in DPBS) reduced the activation of NF-κB by laser exposure. This reduction by AA was evident at the 6 h and 24 h post-exposure assay time points (Figure 6). At 6 h, the reduction in NF-κB was 43%, and at 24 h, the reduction was 75%, compared to untreated, laser-exposed cells. Interestingly, in cells not exposed to laser, but treated with AA, there was a slight increase in the level of activated NF-κB: approximately a 20% increase at 6 h, and a 3-fold increase at 24 h.

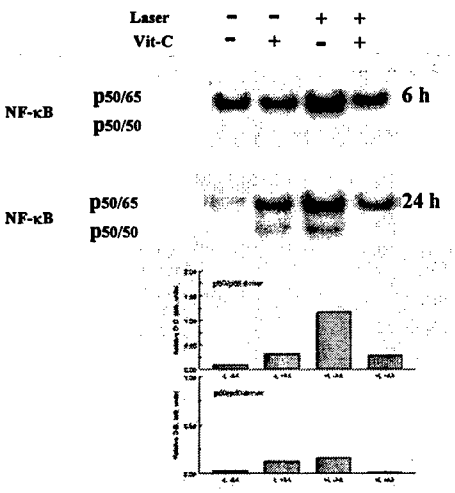

Figure 6. AA pretreatment of RPE cells reduces NF-κB activation by laser. RPE cells were incubated in 500 μM AA prior to laser exposure. The amount of NF-κB in the nuclear extracts was reduced, especially at the 24 h time point. AA treatment by itself appeared to increase the amount of p50/p65 dimer in the control cells. Results of densitometric scans are shown below each lane in the EMSA gel (upper set of bars: p50/p65 dimer; lower set of bars: p50/p50 dimer).

DISCUSSION

NF-κB as an indicator of photo-oxidative and thermal stress

The CW laser irradiation used in this study stressed the hTERT-RPE cells, as evidenced by the activation of NF-κB, which is generally an indicator of oxidative stress or a response to a pro-inflammatory signal, such as a cytokine.[48] The laser irradiance used in these experiments has been demonstrated previously to produce endpoints associated with oxidative damage, including depletion of antioxidants,[49] carbonyl adducts to cellular proteins,[45] and peroxidation of fatty acids.[50] Although the laser exposure paradigm was designed to minimize temperature transients in the target RPE cells, the question of the effect of thermal stress on the cells may be raised. In general, hyperthermia, or heat shock, has been found to decrease or inhibit the activation of NF-κB,[51, 52] although some neural tissues have been reported to show an increase.[53] Heat shock may reduce the levels of NF-κB by producing insolubilization of IκK.[54] Nevertheless, because the moderate laser exposure irradiance used in this work, 0.5 W/cm^2, was below the level generally considered to produce thermal tissue damage, and yet produced an upregulation of NF-κB in RPE cells, we concluded that the primary effect of the laser exposure was to induce photo-oxidative stress.

Lack of effect of thiol-based antioxidants

A surprising finding was that the thiol antioxidants, NAC and PDTC, did not inhibit the NF-κB activation caused by laser exposure. Many reports have found that one or both of these agents, as well as other thioreducing agents, interfere with part of the transcription factor signaling cascade.[34,55] The ability of antioxidants to prevent activation of NF-κB has led to the general hypothesis that reactive oxygen species (ROS) are somehow involved in triggering the phosphorylation and degradation of the IκB inhibitory subunit, thereby releasing the active dimer component.[29] It is to be noted, however, in many studies the inducing agent for NF-κB is a pro-inflammatory cytokine, such as tumor necrosis factor (TNFα), an oxidizing chemical, or other agent that directly interacts with receptor proteins in the plasma cell membrane.[56] Although thiol reducing agents were supposed to have prevented the generation of ROS, a recent study has shown that the likely mechanisms of action of these agents are unrelated to their antioxidant activity. For example, NAC was shown to reduce the binding efficiency of TNFα with its membrane receptor, and PDTC reduced the efficiency of ubiquitin ligase, which is an

enzyme involved in the inactivation of IκB.[57] The lack of effect of the thiol reducing agents against photo-oxidative stress indicates that the laser radiation is interacting with yet another cellular component to produce the transcription factor response.

The RPE cell melanosome as the site for generation of photo-oxidative stress

In contrast to the thiol-based antioxidants, AA pretreatment was found to be highly effective in reducing activation of NF-κB. This observation, combined with the fact that the hTERT-RPE cells are able to synthesize melanin pigment in culture,[58] raises the possibility that the pigment granules are the site of oxidative stress in these cells. At the time these experiments were conducted, the hTERT-RPE cells were noted to have pigment granules (pigmentation was visible in the cell pellets). The ability of AA, but not thiol-based antioxidants, to quench light-activated free radical reactions of melanin was noted in previous work.[47] The failure of thiol-based antioxidants was ascribed to the higher oxidation potential of the -SH (thiol) group, +920 mV, compared to that of ascorbic acid, +320 mV. Thus, if the action of the Argon-ion CW laser exposure was to excite reactive melanin free radicals which, left unquenched, would produce oxidative damage at specific cellular sites, then AA would be expected to reduce these effects, while the thiol-based antioxidants would not. These observations support our hypothesis that the cytoplasmic pigment granules are the locus for laser-induced oxidative interactions in the RPE cell.

The ability of AA to reduce the activation of NF-κB also raises an interesting speculation about the difference between oxidative stress produced by molecular or chemical agents, and that produced by light exposure. In the case of TNFα-mediated induction of NF-κB, the presumptive ROS are produced by the stimulation of biochemical pathways, such as Rac/NADPH oxidase, Rac being a GTP-binding protein involved in many signaling cascades.[57] The production of ROS after TNFα involves activation of energy-dependent enzymatic reactions. In contrast, the direct effect of light on melanin to produce reactive free radicals does not require additional energy, nor are other enzymatic pathways necessarily involved (but may be affected).[50] Thus, suitable antioxidants may directly quench ROS produced by photo-oxidative mechanisms, and may potentially have a therapeutic role in reducing light-induced damage in tissues, such as the retina and RPE. It is yet unclear if NF-κB plays a pro- or anti-apoptotic role in the RPE. Recent work has shown that RPE cells (not hTERT-RPE, but another human-derived cell line) remain

resistant to TNFα-induced apoptosis, despite carrying a mutant, non-degrading IκB that strongly inhibits NF-κB.[59] In the present work, the hTERT-RPE cells exhibited very little apoptosis following the laser exposure. Whether these cells' survival was due to activation of NF-κB, or to some other factor, remains to be demonstrated.

REFERENCES FOR SECTION TWO

1. R.D. Glickman, "Phototoxicity to the retina: Mechanisms of damage," *Int. J. Toxicol.,* **21,** pp. 473-490, 2002.
2. W.T. Ham Jr, R.G. Allen, L. Feeney-Burns, M.F. Marmor, L.M. Parver, P.H. Proctor, D.H. Sliney, and M.L. Wolbarsht, "The involvement of the retinal pigment epithelium (RPE)," in *Optical Radiation and Visual Health,* M. Waxler Ed., pp. 43-67, CRC Press, Boca Raton, FL, 1986.
3. D.T. Organisciak, R.A. Darrow, L. Barsalou, R.M. Darrow, and L.A. Lininger, "Light-induced oxidative damage and apoptosis in the retina," *Invest. Ophthalmol. Visual. Sci.,* **38 (ARVO Suppl.),** pp. S1028, 1997.
4. C. Reme, J. Reinboth, M. Clausen, and F. Hafezi, "Light damage revisited: converging evidence, diverging views?" *Graefes. Arch. Clin. Exp. Ophthalmol.,* **234,** pp. 2-11, 1996.
5. J.E. Roberts, "Ocular phototoxicity," in *Dermatotoxicology,* F.N. Marzuli Ed., pp. 307-313, Taylor and Francis, Washington, D.C., 1996.
6. S.L. Jacques, "Laser-tissue interactions. Photochemical, photothermal, and photomechanical," *Surg. Clin. North Am.,* **72,** pp. 531-558, 1992.
7. W.R. Elliott, H. Zwick, P. Edsall, M. Reddix, and B.E. Stuck, "Oxidative stress in retinal photoreceptors after acute laser lesion: 2,7- dichlorodihydrofluorescein diacetate in the small eye," *Invest. Ophthalmol. Visual. Sci.,* **40(ARVO Suppl),** pp. S955, 1999.
8. B.S. Gerstman and R.D. Glickman, "Activated rate processes and a specific biochemical mechanism for explaining delayed laser induced thermal damage to the retina," *J. Biomed. Opt.,* **4,** pp. 345-351, 1999.
9. K. Konig, Y. Tadir, P. Patrizio, M.W. Berns, and B.J. Tromberg, "Effects of ultraviolet exposure and near infrared laser tweezers on human spermatozoa," *Hum. Reprod.,* **11,** pp. 2162-2164, 1996.

10. C.P. Lin, M.C. Lynch, and I.E. Kochevar, "Reactive oxidizing species produced near the plasma membrane induce apoptosis in bovine aorta endothelial cells," *Exp. Cell Res.*, **259,** pp. 351-359, 2000.
11. M. Karin, T. Takahashi, P. Kapahi, M. Delhase, Y. Chen, C. Makris, D. Rothwarf, V. Baud, G. Natoli, F. Guido, and N. Li, "Oxidative stress and gene expression: the AP-1 and NF-kappaB connections," *Biofactors,* **15,** pp. 87-89, 2001.
12. P. Herrlich, P. Angel, H.J. Rahmsdorf, U. Mallick, A. Poting, L. Hieber, C. Lucke-Huhle, and M. Schorpp, "The mammalian genetic stress response," *Adv. Enzyme Regul.,* **25,** pp. 485-504, 1986.
13. P. Herrlich, K. Bender, A. Knebel, F.D. Bohmer, S. Gross, C. Blattner, H.J. Rahmsdorf, and M. Gottlicher, "Radiation-induced signal transduction. Mechanisms and consequences," *C. R. Acad. Sci. III.,* **322,** pp. 121-125, 1999.
14. F.E. Chen and G. Ghosh, "Regulation of DNA binding by Rel/NF-kappaB transcription factors: structural views," *Oncogene,* **18,** pp. 6845-6852, 1999.
15. T.D. Gilmore, "The Rel/NF-kappaB signal transduction pathway: introduction," *Oncogene,* **18,** pp. 6842-6844, 1999.
16. M. Karin, "How NF-kappaB is activated: the role of the IkappaB kinase (IKK) complex," *Oncogene,* **18,** pp. 6867-6874, 1999.
17. M. Karin, Y. Yamamoto, and Q.M. Wang, "The IKK NF-kappa B system: a treasure trove for drug development," *Nat. Rev. Drug Discov.,* **3,** pp. 17-26, Jan. 2004.
18. H.L. Pahl, "Activators and target genes of Rel/NF-kappaB transcription factors," *Oncogene,* **18,** pp. 6853-6866, 1999.
19. A.A. Beg and D. Baltimore, "An essential role for NF-kappaB in preventing TNF-alpha-induced cell death," *Science,* **274,** pp. 782-784, 1996.
20. X. Hu, M. Tang, A.B. Fisher, N. Olashaw, and K.S. Zuckerman, "TNF-alpha-induced growth suppression of CD34+ myeloid leukemic cell lines signals through TNF receptor type I and is associated with NF-kappa B activation," *J. Immunol.,* **163,** pp. 3106-3115, 1999.
21. N. Mohan and M.L. Meltz, "Induction of nuclear factor kappa B after low-dose ionizing radiation involves a reactive oxygen intermediate signaling pathway," *Radiation Research,* **140,** pp. 97-104, 1994.

22. S.J. Lee, A. Dimtchev, M.F. Lavin, A. Dritschilo, and M. Jung, "A novel ionizing radiation-induced signaling pathway that activates the transcription factor NF-kappaB," *Oncogene,* **17,** pp. 1821-1826, 1998.

23. U. Raju, G.J. Gumin, and P.J. Tofilon, "NF kappa B activity and target gene expression in the rat brain after one and two exposures to ionizing radiation," *Radiat Oncol. Investig.,* **7,** pp. 145-152, 1999.

24. M.M. Simon, Y. Aragane, A. Schwarz, T.A. Luger, and T. Schwarz, "UVB light induces nuclear factor kappa B (NF kappa B) activity independently from chromosomal DNA damage in cell-free cytosolic extracts," *J. Invest. Dermatol.,* **102,** pp. 422-427, 1994.

25. M. Los, H. Schenk, K. Hexel, P.A. Baeuerle, W. Droge, and K. Schulze-Osthoff, "IL-2 gene expression and NF-kappa B activation through CD28 requires reactive oxygen production by 5-lipoxygenase," *EMBO J.,* **14,** pp. 3731-3740, 1995.

26. G.F. Vile, A. Tanew-Ilitschew, and R.M. Tyrrell, "Activation of NF-kappa B in human skin fibroblasts by the oxidative stress generated by UVA radiation," *Photochem. Photobiol.,* **62,** pp. 463-468, 1995.

27. N. Li and M. Karin, "Ionizing radiation and short wavelength UV activate NF-kappaB through two distinct mechanisms," *Proc. Natl. Acad. Sci. U. S. A.,* **95,** pp. 13012-13017, 1998.

28. Y. Devary, C. Rosette, J. DiDonato, and M. Karin, "NF-kB activation by ultraviolet light not dependent on a nuclear signal," *Science,* **261,** pp. 1442-1445, 1993.

29. L. Flohe, R. Brigelius-Flohe, C. Saliou, M.G. Traber, and L. Packer, "Redox regulation of NF-Kappa B," *Free Radic. Biol. Med.,* **22,** pp. 1115-1126, 1997.

30. S.W. Ryter and C.J. Gomer, "Nuclear factor kappa B binding activity in mouse L1210 cells following photofrin II-mediated photosensitization," *Photochem. Photobiol.,* **58,** pp. 753-756, 1993.

31. S. Legrand-Poels, V. Bours, B. Piret, M. Pflaum, B. Epe, B. Rentier, and J. Piette, "Transcription factor NF-kappa B is activated by photosensitization generating oxidative DNA damages," *J. Biol. Chem.,* **270,** pp. 6925-6934, 1995.

32. D.J. Granville, C.M. Carthy, H. Jiang, J.G. Levy, B.M. McManus, J.Y. Matroule, J. Piette, and D.W. Hunt, "Nuclear factor-kappaB activation by the photochemotherapeutic agent verteporfin," *Blood,* **95,** pp. 256-262, 2000.

33. T. Hayashi, Y. Ueno, and T. Okamoto, "Oxidoreductive regulation of nuclear factor kappa B. Involvement of a cellular reducing catalyst thioredoxin," *J. Biol. Chem.*, **268,** pp. 11380-11388, 1993.

34. H. Schenk, M. Klein, W. Erdbrugger, W. Droge, and K. Schulze-Osthoff, "Distinct effects of thioredoxin and antioxidants on the activation of transcription factors NF-kappa B and AP-1," *Proc. Natl. Acad. Sci. U. S. A.*, **91,** pp. 1672-1676, 1994.

35. K. Schulze-Osthoff, H. Schenk, and W. Droge, "Effects of thioredoxin on activation of transcription factor NF-kappa B," *Methods. Enzymol.*, **252,** pp. 253-264, 1995.

36. M. Barkett and T.D. Gilmore, "Control of apoptosis by Rel/NF-kappaB transcription factors," *Oncogene,* **18,** pp. 6910-6924, 1999.

37. M.P. Mattson, Y. Goodman, H. Luo, W. Fu, and K. Furukawa, "Activation of NF-kappaB protects hippocampal neurons against oxidative stress-induced apoptosis: evidence for induction of manganese superoxide dismutase and suppression of peroxynitrite production and protein tyrosine nitration," *J. Neurosci. Res.*, **49,** pp. 681-697, 1997.

38. M. Grilli, M. Pizzi, M. Memo, and P. Spano, "Neuroprotection by aspirin and sodium salicylate through blockade of NF- kappaB activation," *Science,* **274,** pp. 1383-1385, 1996.

39. A. Schneider, A. Martin-Villalba, F. Weih, J. Vogel, T. Wirth, and M. Schwaninger, "NF-kappaB is activated and promotes cell death in focal cerebral ischemia," *Nat. Med.*, **5,** pp. 554-559, 1999.

40. R.R. Krishnamoorthy, M.J. Crawford, M.M. Chaturvedi, S.K. Jain, B.B. Aggarwal, M.R. Al-Ubaidi, and N. Agarwal, "Photo-oxidative stress down-modulates the activity of nuclear factor- kappaB via involvement of caspase-1, leading to apoptosis of photoreceptor cells," *J. Biol. Chem.*, **274,** pp. 3734-3743, 1999.

41. M.J. Crawford, R.R. Krishnamoorthy, V.L. Rudick, R.J. Collier, M. Kapin, B.B. Aggarwal, M.R. Al-Ubaidi, and N. Agarwal, "Bcl-2 overexpression protects photooxidative stress-induced apoptosis of photoreceptor cells via NF-kappaB preservation," *Biochem. Biophys. Res. Commun.*, **281,** pp. 1304-1312, 2001.

42. S. Legrand-Poels, S. Schoonbroodt, J.Y. Matroule, and J. Piette, "Nf-kappa B: an important transcription factor in photobiology," *J. Photochem. Photobiol. B, Biol.*, **45,** pp. 1-8, 1998.

43. A.G. Bodnar, M. Ouellette, M. Frolkis, S.E. Holt, C.P. Chiu, G.B. Morin, C.B. Harley, J.W. Shay, S. Lichtsteiner, and W.E. Wright, "Extension of life-span by introduction of telomerase into normal human cells," *Science,* **279,** pp. 349-352, 1998.

44. X.R. Jiang, G. Jimenez, E. Chang, M. Frolkis, B. Kusler, M. Sage, M. Beeche, A.G. Bodnar, G.M. Wahl, T.D. Tlsty, and C.P. Chiu, "Telomerase expression in human somatic cells does not induce changes associated with a transformed phenotype," *Nat. Genet.,* **21,** pp. 111-114, 1999.

45. R.D. Glickman, "The origin of photo-oxidative stress in the aging eye," *Prog. Brain. Res.,* **131,** pp. 699-712, 2001.

46. S. Mohan, N. Mohan, A.J. Valente, and E.A. Sprague, "Regulation of low shear flow-induced HAEC VCAM-1 expression and monocyte adhesion," *Am. J. Physiol.,* **276,** pp. C1100-C1107, 1999.

47. K.W. Lam and R.D. Glickman, "Prevention of light-induced free radical production from melanin granules by ascorbic acid," in *Oxygen Radicals (International Conference on Oxygen Radicals, Nov. 1991, Kyoto, Japan),* K. Yagi Ed., pp. 633-636, Elsevier Science Publishers, Amsterdam, 1992.

48. R.G. Allen and M. Tresini, "Oxidative stress and gene regulation," *Free Radic.Biol.Med.,* **28,** pp. 463-499, Feb 1. 2000.

49. R.D. Glickman, R. Sowell, and K.W. Lam, "Kinetic properties of light-dependent ascorbic acid oxidation by melanin," *Free Radic. Biol. Med.,* **15,** pp. 453-457, 1993.

50. A.E. Dontsov, R.D. Glickman, and M.A. Ostrovsky, "Retinal pigment epithelium pigment granules stimulate the photo-oxidation of unsaturated fatty acids," *Free Radic. Biol. Med.,* **26,** pp. 1436-1446, 1999.

51. C.L. Li, X.Y. Wang, J. Shao, J.S. Zhang, W.G. Feng, Y.B. Wang, and Z.L. Chang, "Heat shock inhibits IL-12 p40 expression through NF-kappa B signalling pathway in murine macrophages," *Cytokine,* **16,** pp. 153-159, Nov 21. 2001.

52. H.R. Wong, M.A. Ryan, I.Y. Menendez, and J.R. Wispe, "Heat shock activates the I-kappaBalpha promoter and increases I-kappaBalpha mRNA expression," *Cell Stress Chaperones,* **4,** pp. 1-7, Mar. 1999.

53. P. Maroni, P. Bendinelli, L. Tiberio, F. Rovetta, R. Piccoletti, and L. Schiaffonati, "In vivo heat-shock response in the brain: signalling pathway and transcription factor activation," *Brain Res. Mol. Brain Res.*, **119,** pp. 90-99, Nov 6. 2003.

54. K.H. Lee, Y.H. Hwang, C.T. Lee, Y.W. Kim, S.K. Han, Y.S. Shim, and C.G. Yoo, "The heat-shock-induced suppression of the IkappaB/NF-kappaB cascade is due to inactivation of upstream regulators of IkappaBalpha through insolubilization," *Exp. Cell Res.*, **299,** pp. 49-56, Sep 10. 2004.

55. J.C. Epinat and T.D. Gilmore, "Diverse agents act at multiple levels to inhibit the Rel/NF-kappaB signal transduction pathway," *Oncogene,* **18,** pp. 6896-6909, 1999.

56. T. Wang, X. Zhang, and J.J. Li, "The role of NF-kappaB in the regulation of cell stress responses," *Int. Immunopharmacol.*, **2,** pp. 1509-1520, Oct. 2002.

57. M. Hayakawa, H. Miyashita, I. Sakamoto, M. Kitagawa, H. Tanaka, H. Yasuda, M. Karin, and K. Kikugawa, "Evidence that reactive oxygen species do not mediate NF-kappaB activation," *EMBO J.*, **22,** pp. 3356-3366, Jul 1. 2003.

58. L. Rambhatla, C.P. Chiu, R.D. Glickman, and C. Rowe-Rendleman, "In vitro differentiation capacity of telomerase immortalized human RPE cells," *Invest. Ophthalmol. Visual. Sci.*, **43,** pp. 1622-1630, 2002.

59. P. Yang, B.S. McKay, J.B. Allen, and G.J. Jaffe, "Effect of NF-kappa B inhibition on TNF-alpha-induced apoptosis in human RPE cells," *Invest. Ophthalmol. Vis. Sci.*, **45,** pp. 2438-2446, Jul. 2004.

SECTION THREE

Non-invasive thermography of laser-induced hyperthermia using magnetic resonance

INTRODUCTION

Recently, there has been renewed interest in using laser heating to induce localized hyperthermia to treat cancer and other diseases.[1-3] Local hyperthermia can be used for a wide variety of medical interventions such as heart arrhythmias[4] and treatment of solid and vascular tumors, as well as other vascular anomalies of various etiology of the retina and choroid.[5] Generally, photothermal therapy does not produce as much widespread damage as does radiation therapy, e.g. gamma and beta radiation.[6] Therefore photothermal therapy has been recommended as the treatment method of choice for small melanomas situated close to the macula or optic nerve.[5] Such treatment of tumors in the eye (e.g. retinoblastomas and malignant melanomas), utilizing near infrared laser irradiation at the target tissue through the pupil, is called Transpupillary Thermotherapy (TTT), which was introduced by Oosterhuis.[7] The near infrared range of electromagnetic radiation 800-810 nm laser, is the best for such procedures because of the good optical penetration properties of this radiation in the ocular tissue.[6]

The object of thermal treatment is to provide adequate heating to destroy the entire target volume while sparing adjacent normal structures. Interestingly, it has been reported that tumor tissue is more sensitive to increased temperature than is normal tissue.[8] In the TTT treatment, strict confinement of the extent of photothermal damage is critical, because such lesions are frequently located close to the macula or optic nerve as well as retinal pigment epithelium and choroid.[6] Heat conduction through diffusion and perfusion processes may vary locally as a function of tissue architecture, tissue composition, local physiological parameters, and temperature itself.

Thus, there is a need for optimal photothermal treatment where optimal irradiation therapy should take into account the distribution of both radiant and thermal energy throughout the volume of the treated organ or tissue. Optimizing the variable parameters will maximize the effectiveness of the hyeperthermia treatment. Magnetic resonance imaging (MRI) has recently enabled a noninvasive method to measure temperature changes in irradiated tissue, which is more suitable and

advantageous in clinical use than conventional feedback temperature monitoring using a series of thermistor probes. It also minimizes stress on the patient, and reduces the possibility of confounding interactions between the laser radiation and the temperature sensors.[9-11] Magnetic resonance thermal imaging depends on several parameters that are known to be temperature dependent such as the relaxation time, the diffusion coefficient, and the proton resonance frequency.[12,13] The excellent linearity and near-independence with respect to tissue type, together with good temperature sensitivity, make proton resonance frequency (PRF) based temperature MRI the preferred choice of many applications.

In this investigation we carried out measurements of laser-induced temperature changes in an ocular phantom using the PRF based method to evaluate its suitability for ophthalmic applications. This method was able to produce three-dimensional temperature measurements with sufficient spatiotemporal resolution for practical measurements in the eye. Because of local differences in heat conduction and energy absorption, three-dimensional real-time temperature mapping would be ideal. A numerical model based on classical solution of the heat diffusion equation was used to calculate temperature distribution in the phantom irradiated by a laser beam at near infrared wavelength (806 nm), taking the redistributive scattering into account, which was then compared to measured empirical data.

METHODS

Ocular Phantoms

Two types of phantoms were used during the course of this research. A uniform ocular phantom was constructed by filling a 22-mm diameter, cylindrical glass cuvette with either clear, 1% agarose (Sigma Chemical Co., St. Louis, MO), or 1% agarose containing a uniform suspension of melanosomes isolated from bovine retinal pigment epithelium (RPE) as previously described.[14] The agarose was dissolved in distilled water, heated to 60 °C, poured into the cuvette, and allowed to gel. The uniform phantoms were used only for calibration of the MRT temperature response, as described below ("MR Thermography"). For experiments involving laser radiation, a non-uniform phantom containing a thin layer of melanin was constructed using a 10-cc Pyrex glass beaker, also of approximately 22-mm diameter. The melanin layer was formed by mixing a suspension of

bovine RPE melanosomes in agarose at a granule density estimated to be similar to that in native RPE, i.e. approximately 10^{10} melanin gran/ml.[14] This melanosome-agarose suspension was sandwiched and allowed to gel between two microscope cover slips, forming a layer of 1.5 mm thickness. The sandwich was placed in the middle of the beaker, and clear agarose was poured in around it.

Infrared Laser Irradiation of Phantoms

The laser source used in this study was an HPM-F1 laser diode module with a built-in fiber launch, that produced 1 watt CW maximum output power at 806 nm (Power Technology Corp, Little Rock, AK). The experimental optical and temperature-recording arrangement is shown in Figure 1. The laser console was situated about 4.5 meters away from the center of the MR magnetic field. The laser emission was delivered into the cavity of the MR instrument using a 5-meter long, 600 μm diameter core, multimode optical fiber (Oz Optics, Carp, Ontario, Canada). An in-line, fiber optic variable attenuator (Oz Optics) controlled the laser power delivered to the phantom. Two lenses were used to collimate (L1, 50 mm focal length) and focus (L2, 11 mm focal length) the laser beam on the phantom target inside the MR cavity, as shown in Figure 1. The lenses and fiber optic were mounted and aligned in a non-magnetic holder. Separately, the focused laser spot size at the target was imaged with a BeamView Analyzer PC laser beam profiler (Coherent Inc., Instruments Div., Auburn, CA) and was found to be an approximately Gaussian beam. In these experiments, two laser beam sizes on the target were used: a small spot with $1/e^2$ radius of 0.8 mm, and a large spot with $1/e^2$ radius of 2.4 mm.

The laser power at the target position was measured with an EPM 1000 energy/power meter equipped with a MP3 thermopile detector head (Molectron, Eugene OR). Depending on the experiment, the target irradiance was varied over the range of 2.4 - 21.6 W/cm^2. This was determined by placing the power detector at the position of the phantom, and taking in account the small attenuation due to the glass vessel and the agarose. Laser beam alignment was visually checked using a Find-R-Scope infrared viewer (FJW Optical Systems, Palatine, IL) to ensure that the laser beam was centered in the ocular phantom.

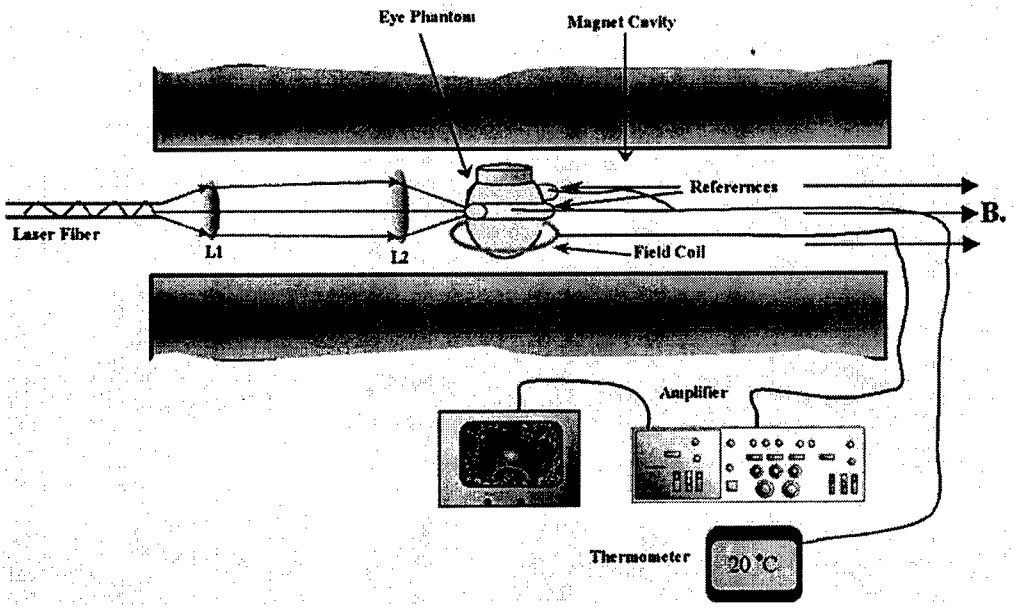

Figure 1. Schematic of the experimental setup. The ocular phantom was placed on a 2-turn 6-cm diameter, circular radiofrequency coil, in the 45-cm bore of a 2T MR imager. Three reference phantoms were placed alongside the main phantom. Independent temperature measurements were made with Vitek temperature probes. The laser was brought into the MR cavity with an optical fiber, and the 806 nm beam was focused into the phantom with lenses L1 and L2. The orientation of the applied magnetic field, B_0, is indicated on the diagram. Phase images wee obtained using a Tecmag Libra console.

MR Thermography

All MRT experiments were performed in the MRI Laboratory of the Research Imaging Center at the University of Texas Health Science Center at San Antonio. Measurements were made using a PRF method similar to that described by Vitkin et al.[15] For MR thermography methods utilizing PRF, the image phase difference is linearly dependent on the change in temperature as follows:

$$\Delta\varphi = \alpha \cdot \gamma \cdot B_0 \cdot TE \cdot \Delta T \qquad (1)$$

where $\Delta\varphi$: phase difference, γ : the gyromagnetic ratio for protons, B_0 : magnetic field strength, α : the thermal coefficient (i.e. the chemical shift), TE: echo time, and ΔT : change in temperature. A two-turn radiofrequency surface coil of 6-cm diameter was used as the transceiver. Images were

obtained using an Oxford Magnet Technology 2T, 45-cm diameter bore, superconducting magnet (Oxfordshire, England), equipped with actively shielded Magnex gradients and a Tecmag Libra console (Tecmag, Houston, TX).

In order to calibrate the MRT measurements in terms of absolute temperature, an experiment was performed with a phantom containing a uniform distribution of melanin granules, constructed as described above ("Ocular Phantoms"). The phantom was heated by passing warm water from an external circulating water bath through Tyvek tubing wrapped around the phantom. When thermal equilibrium was reached, the water flow was stopped. MRT was performed by subtracting the phase images of the ocular phantom at two different temperatures, and constructing a phase difference map, from which the temperature difference was calculated using equation (1). To correct for phase drifts due to ambient temperature changes unrelated to temperature shifts in the ocular phantom, thermally isolated reference phantoms, consisting of small tubes of agarose, were placed adjacent to the ocular phantom. On the assumption that the phase in the image of the reference phantoms remained constant, the relative temperature change map of the ocular phantom was corrected by comparison to the phase of three points in the image of the reference phantoms (three points allowed a image plane to be defined). The reference phantoms had known length, which enabled the correction of three-dimensional images. Gradient echo images were obtained at various phantom temperatures. From these images, the value of α (the chemical shift) was found to be 0.0102 ppm/°C, consistent with general PRF temperature measurements for biological tissues.[12] The signal to noise ratio (SNR) for the temperature measurements was calculated as the inverse of the standard deviation of the phase over the region of interest (ROI) in the heated sample. For absolute calibration, the temperatures inside the ocular phantom and in the references were measured independently, with an accuracy of 0.1 °C, using Vitek fiber optic temperature probes (Boulder, CO) placed in the phantoms.

For all laser-induced heating experiments, the layered phantom consisting of a melanin layer embedded in clear agarose as described above, was used. The melanin itself has natural T1 contrast in MRI. The 806 nm light emitted from the diode laser source was not significantly absorbed in the clear agarose, but was almost entirely absorbed and scattered within the melanosome layer (refer to

Figure 3A). This was considered to be a close approximation of the behavior of near infrared light in the vertebrate eye. To obtain a time course of the heating in the phantom, a two-dimensional, gradient echo imaging sequence was used with repetition time (TR) of 210 ms, echo time (TE) of 12 ms, and the flip angle was 40°. Eight slices were acquired with images obtained every 22.9 s. The in-plane resolution was 0.25 mm with a slice thickness of 1.5 mm. Six images were taken before the laser was turned on and these were averaged to provide a phase reference image. Laser-induced heating was applied for 15 - 20 minutes, and images were taken sequentially throughout the exposure period.

A three-dimensional (3D) temperature map was obtained in the melanin-layer phantom, using a 3D gradient echo imaging sequence providing an image of 0.25×0.25×0.25 mm resolution in each direction. In this gradient sequence, TR = 40 ms, TE = 12 ms, and the flip angle = 20°. The time required for a total 3D scan was 8 minutes. A 3D image prior to heating was acquired as the reference image, as well as two 3D images after the laser had been turned on. Acquisition of the first image commenced with the onset of laser exposure (the center of k-space was after 4 minutes), while the second image was acquired after the completion of the laser exposure (the center of k-space was after 13 minutes). Three-dimensional scans were acquired during heating of the phantom with the small (0.8 mm radius) as well as the large (2.4 mm radius) laser beam spot sizes.

Image Analysis

Phase maps were reconstructed from adjusted phase drifts using IDL (Interactive Data Language from Research Systems, Inc., Boulder, CO), using the three-point phase correction method described in section 2.3, and by previous authors.[11,22] Temperature maps were then calculated using equation (1).

Infrared Imaging

Infrared photography was performed using a Sony F717 digital camera set to its "Nightshooting" operational mode, i.e. with the CCD imager set to record only near infrared light. Images were taken of the phantom during 806 nm laser irradiation, and then transferred to a personal computer for processing and display.

Thermal Model

A basic model for the transient thermal tissue response to continuous diode laser output was used to predict the temperature rise and to compare it with the MRT measured values. The thermal model accounted for the effect of light scattering, which is predominant in the case of melanized tissue. In previous work, the inverse adding doubling (IAD) method[16] was used to determine optical properties of RPE melanin. The scattering coefficients were found to be much higher than the absorption coefficients of melanin at visible wavelengths,[17,18] and this relationship would be expected to be similar in the near infrared, although the relative magnitude of each coefficient would be lower than the corresponding visible wavelength values.[18] Moreover, the exact values depend slightly on the concentration of melanin in the phantom. Thus, when compared with visible wavelength lasers, lasers emitting in the near infrared (e.g. 806 nm wavelength) will experience less scattering and correspondingly increased transmission through non-transparent (turbid) media.

Some simplifying assumptions were made. The thermal radiation away from the phantom walls was neglected, and material constants were taken to be uniform and time independent. The optical and properties of the material were also considered to remain constant during temperature elevation.

If the incident intensity, $I_o(r)$ (Watt/cm^2), of a cylindrical, symmetric laser beam penetrates the surface, then the intensity of the direct beam, I^B follows as in Beer's law:

$$I^B(r,z) = I_O(r)\exp(-\mu z) \qquad (2)$$

where

$$\mu = \mu_a + \mu_s \qquad (3)$$

and μ is the extinction coefficient, μ_a is the (direct) absorption coefficient of radiation, and μ_s is scattering coefficient (redistribution) of radiation out of the beam. However, the intensity of scattering radiation, I^S, at (r,z) is the sum of direct intensity as result of depolarization and other randomizing effects, and can be written as for cylindrical symmetry[19,20]:

$$I^s(r,z) = \frac{\mu_s}{4\pi} \int_0^\infty r'dr' \int_0^{2\pi} d\theta'' \int_0^D dz' \times \frac{I_0(r')\exp(-\mu z' - l\mu_s)}{l^2} \quad (4)$$

where l is the distance between points (i.e. intensity of radiation arriving at (r',θ',z'), to which light has been scattered from (r,0,z) with coefficient μ_s in cylindrical co-ordinates).

From the input optical parameters, the effective penetration depth δ_{eff} can be written:

$$\delta_{eff} = \frac{1}{\sqrt{3\mu_a[\mu_a + (1-g)\mu_s]}} \quad (5)$$

where g is the anisotropy factor (dimensionless).

The temperature response of tissue to a laser radiation source S is governed by the following heat equation:[21]

$$\rho c \frac{\partial T}{\partial t} = K\nabla^2 T + S \quad (6)$$

where T is temperature, ρ is density (kg/m^3), c is the specific heat (J/kg • °K) of the substance, and K is the thermal conductivity (W/m • °K). The source function can be expressed as:

$$S(r,z,t) = \alpha[I^B(r,z,t) + I^s(r,z,t)] \quad (7)$$

This enters the heat equation linearly as a driving function. The laser beam profile is considered as a Gaussian profile with laser beam waist r_o:

$$I_o(r) = I_o \exp[-(r/r_o)^2] \quad (8)$$

This distribution corresponds to total input power :

$$P = \pi r_0^2 I_o \qquad (9)$$

An analytical solution of the heat differential equation by using the Eigenfunction with the relation between I^s and I^B has been discussed in detail.[19] In the present application, these problems were solved numerically by using Mathcad (Mathsoft Engineering, Cambridge, MA); the results of the computation were displayed graphically, as will be shown below.

RESULTS

Measurement of Heating Time course

Temperature profiles within the layered phantom during continuous application of the 806 nm diode laser were measured using MRT, and compared to the theoretical values predicted from the heat diffusion model. The optical properties assigned to the melanin layer phantom were as follows: (scattering coefficient) $\mu_s \sim 11.4\ cm^{-1}$, (absorption coefficient) $\mu_a \sim 0.55\ cm^{-1}$, and (anisotropy factor) $g = 0.92$. The thermal constants were taken as $\rho c = 4.4\ J/cm^3 \cdot {}^\circ C$ (i.e. as for water), and $K = 7 \times 10^{-3}$ $W/cm \cdot {}^\circ C$, and were assumed to be uniform throughout the phantom.

During steady exposure, the time course of heating was obtained by serial MRT measurements as described above ("MR Thermography"). The layered phantom reached 75% thermal equilibrium after a laser exposure of 25-30 seconds, as shown in Figure 2, with a target irradiance of 21.6 W/cm^2 at the center of the phantom, and the 0.8 mm radius ($1/e^2$) laser beam. The experimental example shows that the steady state temperature reached within 75 sec was 23 °C above the initial baseline, which is very high relative to the temperature achieved in typical hyperthermia treatment. Also shown in Figure 2 is an estimate of the error in the two-dimensional MRT measurements. Prior to the start of laser heating, the standard deviation of the phase in six consecutive 2D images was 0.047 radians, corresponding to 0.72 °C. This implied that the temperature resolution in the unheated sample was better than 1 degree. During laser heating, however, the signal to noise ratio declined, and the standard deviation of the phase increased, leading to an estimate of measurement

error of 1.4 °C. This is indicated by the error bars in Figure 2 for the time points starting at 75 sec after the onset of laser exposure, i.e. for MRT measurements made during steady-state heating.

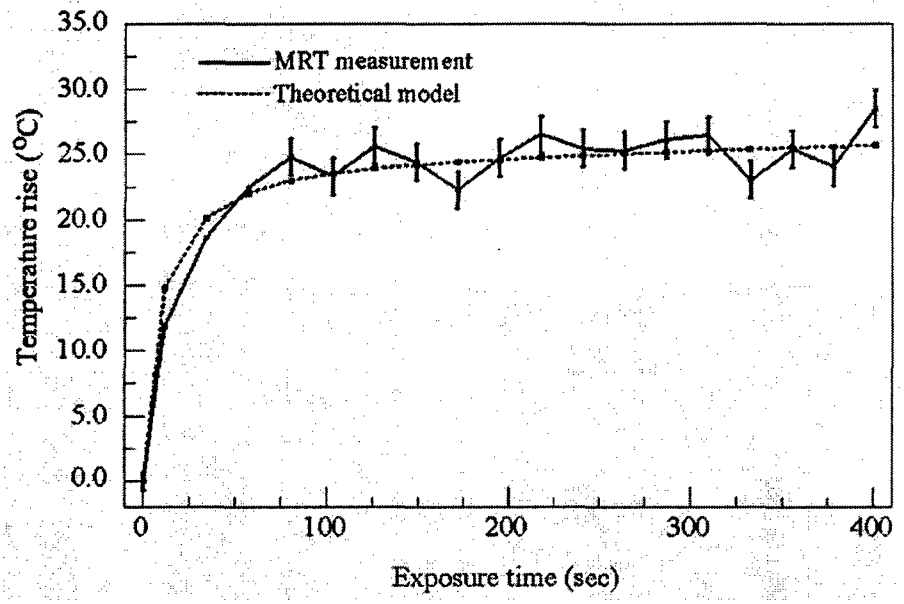

Figure 2. Heating time course in the layered phantom during CW infrared laser exposure, as measured with MRT. The solid line shows the temperature change at the hottest point in the phantom, within the melanin layer, measured with MRT in sequential images during laser irradiation. The dotted line shows theheating time course predicted by the heat diffusion model. The error bars on the MRT measurements show the standard deviation of the phase measurements, converted to temperatures. Laser heating was applied for 15 min; the temperature measured in the phantom during the first 400 sec of the experiment is shown in this figure. The ordinate shows the temperature increase in the phantom's melanin layer during laser irradiation. Taking into account minor scattering and absorption of the 806 nm laser in the clear agarose portion of the phantom, the target irradiance in the melanin layer was calculated as 21.6 W.cm^2. where the laser beam radius was ($1/e^2$) was 0.8 mm.

Spatial and Thermal Resolution of 2D MRT

Measuring two-dimensional temperature gradients in the layered phantom during infrared laser exposure assessed the spatial resolution of the MRT method. A difference in the spatial temperature gradients due to the non-homogeneity of the melanin layer in the phantom was readily apparent. Infrared imaging revealed the optical propagation of the laser beam through the phantom. The beam propagated with a small amount of scattering and very little absorption through the clear agarose gel, but was highly scattered and absorbed in the melanin layer (Figure 3A). A corresponding MR magnitude image of the phantom is shown for comparison in Figure 3B.

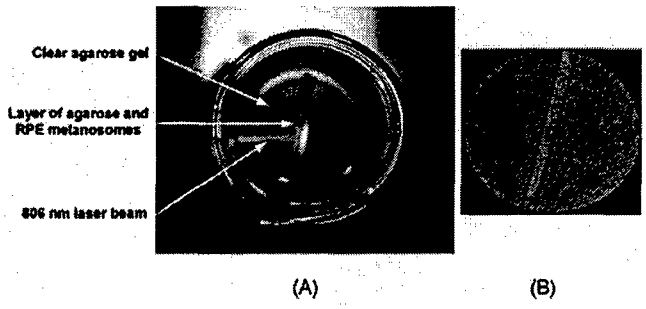

Figure 3. (A) Infrared image taken of the 806 nm laser beam propagating through the layered phantom. The IR image was taken with a Sony F717 camera (IR imaging mode) of the phantom outside of the MR cavity. During the actual experiment, the laser beam was normally incident on the melanin layer. (B) MR magnitude image of the layered phantom. The melanin layer appears brighter than the surrounding clear agarose because of melanin's inherent T1 contrast.

Because of its paramagnetic moment,[23] the melanin layer has higher T1 contrast than the surrounding agarose. Temperature gradients were measured in the layered phantom using MRT during laser exposures delivering sufficient power into the phantom to produce heating (Figure 4). A thermographic image was constructed by obtaining the phase difference between a magnetic resonance image taken prior to the onset of the laser, and one taken during the laser exposure. The thermographic (phase difference) image is shown in Figure 4A. The spatial resolution of the MRT images was determined by the number of image voxels within the physical field of view. The in-plane resolution of the 2D MR images was 0.25 mm. The MRT spatial resolution was sufficient to distinguish between temperature gradients measured within the plane of the melanin layer, and those orthogonal to the layer, as shown in Figure 4B. The gradient within the melanin layer is wider compared to the orthogonal profile. That difference can be explained by the low optical absorption of the laser beam within the clear agarose, in contrast to the high optical absorption – and hence, heating – of the laser beam in the melanin layer.

The theoretical temperature resolution of MRT based on the PRF method may approach 0.1 °C.[12] By using an external water bath to heat the phantom uniformly to a known temperature, the MRT measurements were calibrated so that an absolute temperature could be derived from the temperature-dependent phase changes in the image. In addition, by comparing the agreement of MRT of the water-bath heated phantom, determined from 2D images, with temperature

measurements made with a Vitek probe, an estimate of the accuracy of the method was attained, and was found to be within 0.5 °C, at least for temperature excursions less than 10 °C.

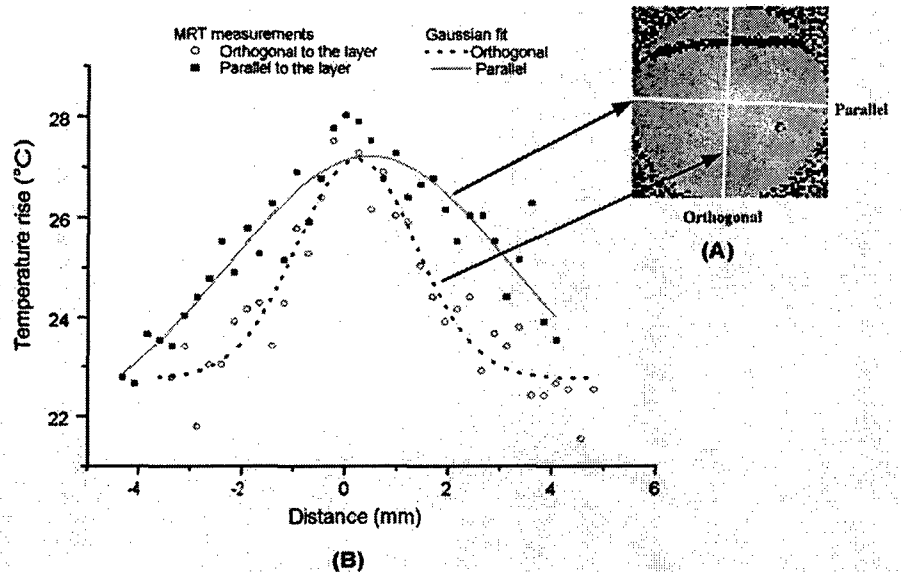

Figure 4. Orthogonal temperature profiles in the layered phantom during laser exposure. (A) The phase image of the phantom during laer-induced heating: the dark band near the top of the image is an artifact in the phase unwrapping algorithm. The white lines in the figure indicate the relative orientations of the temperature gradients with respect to the melanin layer in the phantom. (B) A graph of the temperature gradients in the phantom as a function of displacement from the focal point of the laser beam in the melanin layer. The *filled symbols* represent MRT measurement in a slice extending through the hottest point in the phantom, i.e. within the plane of the melanin layer through the laser focal point; *open symbols* represent MRT measurements in a slice running through the laser focal point, in a plane perpendicular to the melanin layer. Both image slices extended across the entire width of the phantom. Continuous lines through both data sets are best-fit Gaussian functions. The temperature gradient within the melanin layer is broader than the gradient across the layer extending into the clear agarose on each side of the melanin layer, due to the greater scattering and absorption of the laser energy in the melanin granules.

Three-Dimensional Temperature Profiles

Once at the thermal equilibrium, volume image scans were made to construct a three-dimensional thermographic image of steady-state heat flow through the phantom, starting from the focal point of the laser beam where it interacted with the melanin layer. The spatial resolution of the 3D images was 0.25 mm in all three axes. The data sets shown in Figure 5 illustrate the temperature

topography inside the volume of the phantom. It may be appreciated that the temperature gradients follow a Gaussian profile due to the Gaussian distribution of power in the laser beam. The diameter of the laser beam irradiating the phantom also affected the shape of the three-dimensional heating profile. The three-dimensional thermogram resulting from exposure to the 0.8 mm radius laser beam, shown in Figure 5A, is narrower than the thermogram produced by the 2.4 mm radius beam, shown in Figure 5B. The SNR for the three-dimensional magnitude image was 11.5 (calculated as the inverse of the standard deviation of the phase over the ROI). To obtain an estimate of the error in the temperature measurements, the squares of the errors across the image ROI were added, and the square root taken. Converting back to temperature, the derived estimate of error in the 3D data set was ±1.9 degrees.

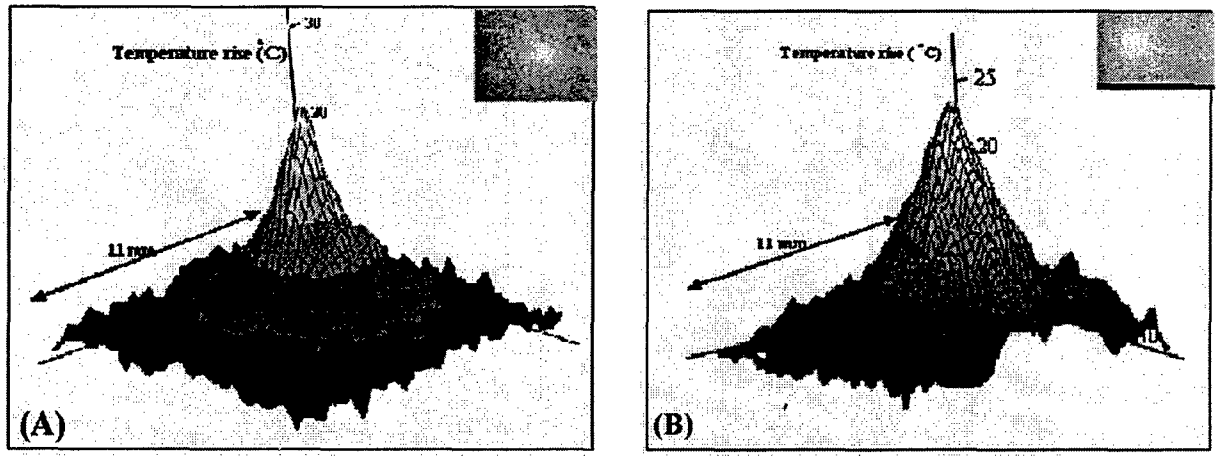

Figure 5. Surface plots taken from three-dimensional maps of the layered phantom during steady-state laser exposure. (A) The thermogram resulting from exposure of the phantom to the 0.8 mm radius laser beam. (B) The thermogram resulting from exposure of the phantom to the 2.4 mm radius laser beam. The inset in the upper right-hand corner of each figure shows the phase difference image (thermogram) of the melanin layer (the image slice was taken within the plane of the melanin layer). The thermograms illustrate the temperature gradients spreading out into the phantom, away from the center of the laser beam incident on the melanin layer. The view of the surface plot is approximately 90° to the axis of the incident laser beam.

Correlation of Thermal Model and MRT Measurements

In order to compare a temperature profile measured by MRT during laser exposure with the heating gradient predicted by the heat diffusion model described in Section 2.4, a two-dimensional image

slice was taken out of the three-dimensional data set shown in Figure 5A. The temperature profile obtained from this image slice is shown in Figure 6 as the discrete points, while the continuous line in Figure 6 shows the temperatures predicted by equation (5). The error bars shown in Figure 6 represent the error estimates derived from the three-dimensional data sets as described above ("Three-Dimensional Temperature Profiles"). The phantom heating was produced by continuous wave laser exposure of 21.6 W/cm^2, 0.8 mm beam radius (1/e^2), and 700 seconds duration. The maximum temperature rise at the center of the phantom was about 32 °C, which was extreme for hyperthermia treatment, but a good test of the ability of MRT to record a large temperature excursion with high resolution. The agreement in Figure 6 between the theoretical and experimental values is quite close. This result indicates that the observed values were well correlated with the predicted values, and that the heat diffusion model is an excellent predictor of heat transfer in such basic applications.

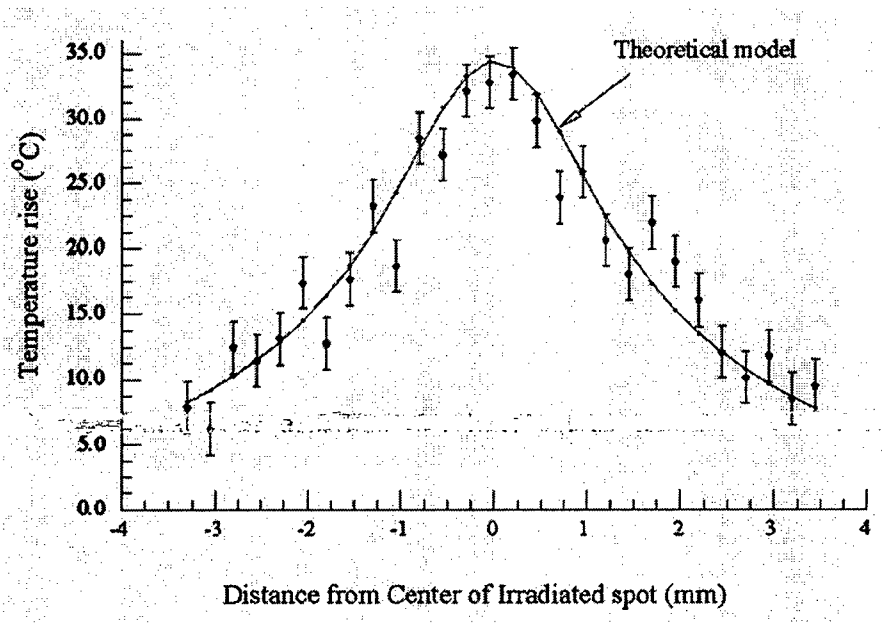

Figure 6. Comparison of the heat diffusion model computational results and the temperature profile measured by MRT within the layered ocular phantom during IR laser exposure. The filled, discrete symbols represent the MRT measurements taken from a central image slice of the 3D data set shown in Figure 5A. The continuous line represents the temperature rise in the phantom predicted by the thermal model as a function of displacement from the center of the laser beam incident on the melanin layer. Error bars on the discrete points are estimates of temperature measurement standard deviation, calculated as described in the section, titled "MR Thermography".

DISCUSSION

Practical Spatial, Temperature, and Temporal Resolution of MRT

The accuracy of the temperature calculations made with MRT depend on several factors, the most important of which is the determination of the thermal coefficient, α. In the present application, for elevations of less than 10 °C produced by passive heating of the uniform phantom with the water bath, the temperature values determined by MRT were compared to measurements made with a Vitek fiber optic probe having an accuracy of 0.1 °C, and usually agreed to within 0.5 °C. The temperature resolution, however, may depend on the magnitude of the temperature excursion. For example, during the more extreme heating produced by the laser exposure, the SNR of the temperature measurements decreased, and for temperature changes of more than 20 °C, the resolution decreased in 2D MRT to about 1.4 °C, and to 1.9 °C for 3D MRT. This implies that the practical temperature resolution of the MRT method decreases with an increase in the relative temperature change in the target, although the resolution is probably better than 1 °C for clinically relevant temperature excursions. Another potential source of error is due to an interaction between the size and orientation of the heat source with the external magnetic field. Peters et al. demonstrated that, with an interstitial laser fiber having a 1-cm long quartz diffuser, there was an orientation-dependent effect on the measured temperature that was ascribed to a change in the volume-magnetic susceptibility of the tissue along the axis of the fiber diffuser.[13,24,25] With a laser beam applied externally, as in the present case, this orientation artifact would be expected to be minor, because the effective heat source in the phantom, i.e. the image of the laser beam, is thin compared to the optical zone absorbing the laser energy, i.e. the melanin layer. In a more complicated target such as the eye (in which the RPE layer containing melanin is very thin), a correction for orientation dependence may have to be introduced. This will be examined in future work.

In terms of spatial resolution, an effective resolution of 0.25 mm was obtained. Given the average thickness of the human retina (350-500 microns), the RPE (20 microns), and the choroid (100-200 microns),[26] the 0.25-mm spatial resolution in the present MRT implementation is sufficient to provide two or three temperature measurement points through the combined thickness of the retina and choroid layers, although insufficient to distinguish retinal and RPE temperature. Nevertheless,

the currently achievable resolution supports the application of MRT to monitor the heating of the target vascular membrane, as well as surrounding retina and RPE, during treatment of choroidal neovascularization by TTT.[1-3] A limitation of TTT at present is that the target temperature required for the optimal therapeutic effect has not been established. Use of MRT for feedback control during TTT could provide critical temperature information to correlate with the resulting tissue responses to the treatment.

Validation of Thermal Models

Experiments in this investigation indicated a good agreement between the calculated data from the basic thermal model and data measured with the MRI technique. Such an agreement depends critically on the physical and optical properties, such as the thermal conductivity, specific heat capacity, density, absorption and scattering coefficients, and the pigmentation and the homogeneity of the tissue, that are entered into the model and control the calculation of both the radiation distribution and the thermal energy distribution. The near infrared laser has been reported to have less scattering effect in pigmented tissue compared to the visible wavelengths, although the scattering is still the dominant process at 806 nm. The effective penetration depth at 806 nm in the melanized layer of our phantom has been calculated from equation (5) to be $\approx$0.7 mm, which is less than the width of the phantom's melanin layer (2 mm thick). Consequently most of the optical heating by the laser radiation at 806 nm was confined in the slab of the melanin layer, consistent with the light propagation revealed with the infrared image shown in Figure 3A. This also will slow the laser-induced heating time in the thick melanin layer of the phantom compared to the thin RPE layer (~10 μm) of the physiological eye. Another factor slowing the heating process in the melanin layer is the size of the phantom. Within the 2.5cm radius of the phantom, more heat will be distributed by diffusion throughout the agarose volume surrounding the melanin layer. But that is analogous to the real eye, where heating the ocular tissue also involves heating the vitreous body.

Variation in the concentration of melanin granules in the absorbing layer will cause variation in the optical properties, which can critically affect the thermal model's ability to predict temperature distribution. To date, there have been few consistent measurements of optical properties of the retinal pigment epithelium (RPE) or choroid layer.[27] Accurate measurements of the optical

properties are critical inputs for heating models, and better validation of thermal models can be done by comparing theoretical predictions of infrared laser heating with MRT measurements using different concentration of melanin granules in absorbing layers of phantom models. Another consideration is that the influence of radiational transport will be less important to the treated volume in the case of long heating time (because of thermal equilibration).

The present model is conceptually straight forward, with further computational frugality achieved by taking simple considerations of boundary conditions. The geometric and thermal assumptions reflect values which limit the accuracy and flexibility of the model. More complex models can be developed for future laser hyperthermia studies using a finite element approach. An advanced model would take into consideration radiational transport in ocular tissue among different layers, such as the RPE and choroid, with different optical and physical properties. In addition blood flow in the choroid would be another factor to consider in *in vivo* studies.

Technical Limitations and Improvements in the Method

The temperature and spatial resolution of the present system appear to be adequate for application to the human eye. The temporal resolution, however, could be improved. There is a tradeoff between temporal, spatial, and temperature resolution. Increasing the resolution of one inevitably reduces the resolution of one or both of the remaining parameters; therefore, the experiment must be designed to maximize the most important parameter. For example, in a study of experimental interstitial laser hyperthermia therapy to the prostate, a single image slice was acquired in 6.7 sec, but with a slice thickness of 5 mm.[28] Certainly, a faster image acquisition rate would be very useful in improving the accuracy of heating time course measurements in the target tissue. It is likely that advances in MR instrumentation will improve overall imaging performance.

Application of MRT to Characterizing the Interaction of IR Laser with Ocular Tissue Components

The MR measurements in the ocular phantom provided a means for directly studying the factors governing the temperature distribution during infrared laser exposure. The physical distribution of the melanin pigment granules, the concentration (or density) of melanosomes in the tissue, and the thickness of the pigmented tissue layer all determined the effective optical zone in which laser-tissue interaction occurred. There were limitations in the ability of the phantom to simulate thermal

interactions likely to occur in the living eye. Practical considerations in the construction of the layered phantom limited its ability to simulate the eye morphology more accurately. For example, the laser-induced heating time course measured in these experiments was considerably slower than the thermal behavior predicted for retina and RPE during laser irradiation.[29,30] Considering that the heat diffusion process will be complicated for a blood-perfused, inhomogeneous organ such as the human eye, MRT provides a non-invasive means for determining *in vivo* the heating time course as well as the equilibrium temperature, both essential for understanding the biological response of the tissue to thermal stress.

The interaction of the 806 nm CW diode laser with melanin is dominated by thermal effects, and depends primarily on photon scattering. For example, the relatively high absorption coefficient of melanin produced a high temperature rise in the small volume of the melanin layer, which caused heat to diffuse throughout the phantom. This effect is illustrated in Figure 4, which shows that the laser radiation was mostly absorbed within the melanin layer, and that heating profiles through the phantom depended on the particular geometry of the absorbing layer in the phantom. Selection of suitable laser parameters for hyperthermia therapy, therefore, will depend on the ability to predict accurately the interaction of the laser beam with the tissue and the resultant heat flows through the treated and adjacent non-treated tissue. Such predictions will require the use of a validated treatment model. The good agreement of the MRT measurements with the predictions of a classical heat diffusion model show that an important use of the method is to validate theoretical models of laser-tissue thermal interaction. One practical embodiment of this ability would be to support the clinical use of a thermal model to plan therapy and optimize the exposure parameters for laser-induced hyperthermia treatment protocols.

REFERENCES FOR SECTION THREE

1. M. A. Mainster and E. Reichel, "Transpupillary thermotherapy for age-related macular degeneration: long-pulse photocoagulation, apoptosis, and heat shock proteins", *Ophthal. Surg. Las.* 31 (5), 359-373 (2000).

2. M. Ip, A. Kroll, and E. Reichel, "Transpupillary thermotherapy", *Seminars in Ophthalmology* 14 (1), 11-18 (1999).

3. E. Reichel, A. M. Berrocal, M. Ip, A. J. Kroll, V. Desai, J. S. Duker, and C. A. Puliafito, "Transpupillary thermotherapy of occult subfoveal choroidal neovascularization in patients with age-related macular degeneration", *Ophthal.* 106 (10), 1908-1914 (1999).

4. S. Levy, "[Biophysical basis and cardiac lesions caused by different techniques of cardiac arrhythmia ablation]. [French]", *Archives des Maladies du Coeur et des Vaisseaux* 88 (10), 1465-1469 (1995).

5. N. Bornfeld, A. Wessing "Photocoagulation of choroidal melanoma", In:*Schachat AP (ed) Retina. Mosby*, St Louis 815-823, (1994).

6. P. Rol, F. Frankhauser, H. Giger, U. Durr, S. Kwasniewska "Transpupillar laser phototherapy for retinal and choroidal tumors: A rational approach", *Graeffe's Arch Exp Ophthalmol*, 238, 249-272, (2000).

7. J.A. Oosterhuis, H.G. Journee-de-Korver, H.M. Kakebeeke-Kemme, J.C. Bleeker "Thranspupillarly thermotherapy in choroidal melanomas", *Arch Ophthalmology* 103, 110-116, (1995).

8. L. J. Anghileri and J. Robert, "Hyperthermia in cancer treatment", *Vol. III, CRC Press*, Boca Raton, FL (1986).

9. A. R. Bleier, F. A. Jolesz, M. S. Cohen, R. M. Weisskoff, J. J. Dalcanton, N. Higuchi, D. A. Feinberg, B. R. Rosen, R. C. McKinstry, and S. G. Hushek, "Real-time magnetic resonance imaging of laser heat deposition in tissue", *Mag. Res. Med.* 21 (1), 132-137 (1991).

10. J. A. de Zwart, P. van Gelderen, D. J. Kelly, and C. T. Moonen, "Fast magnetic-resonance temperature imaging", *Journal of Magnetic Resonance Series B* 112 (1), 86-90 (1996).

11. J. De Poorter, C. De Wagter, Y. De Deene, C. Thomsen, F. Stahlberg, and E. Achten, "Noninvasive MRI thermometry with the proton resonance frequency (PRF) method: in vivo results in human muscle", *Mag. Res. Med.* 33 (1), 74-81 (1995).

12. B. Quesson, J. A. de Zwart, and C. T. Moonen, "Magnetic resonance temperature imaging for guidance of thermotherapy", *J. Magn. Reson. Imag.* 12 (4), 525-533 (2000).

13. R. D. Peters and R. M. Henkelman, "Proton-resonance frequency shift MR thermometry is affected by changes in the electrical conductivity of tissue", *Mag. Res. Med.* 43 (1), 62-71 (2000).

14. A. E. Dontsov, R. D. Glickman, and M. A. Ostrovsky, "Retinal pigment epithelium pigment granules stimulate the photo-oxidation of unsaturated fatty acids", *Free Rad. Biol. Med.* 26 (11/12), 1436-1446 (1999).

15. I. A. Vitkin, J. A. Moriarty, R. D. Peters, M. C. Kolios, A. S. Gladman, J. C. Chen, R. S. Hinks, J. W. Hunt, B. C. Wilson, A. C. Easty, M. J. Bronskill, W. Kucharczyk, M. D. Sherar, and R. M. Henkelman, "Magnetic resonance imaging of temperature changes during interstitial microwave heating: a phantom study", *Med. Physics* 24 (2), 269-277 (1997).

16. S. A. Prahl, M. J. C. van Gemert, and A. J. Welch, "Determining the optical properties of turbid media by using the inverse adding-doubling method", *Appl. Opt.* 32, 559-568 (1993).

17. D. K. Sardar, M. L. Mayo, and R. D. Glickman, "Optical characterization of melanin", *J. Biomed. Opt.* 6 (4), 404-411 (2001).

18. S. L. Jacques, R. D. Glickman, and J. A. Schwartz, "Internal absorption coefficient and threshold for pulsed laser disruption of melanosomes isolated from retinal pigment epithelium," in *Laser-Tissue Interaction VII,* S. L. Jacques, Ed., *Proc. SPIE* 2681, 468-477, SPIE, Bellingham, WA (1996).

19. T. Halldorsson and J. Langerholc, "Thermodynamic analysis of laser irradiation of biological tissue", *Appl. Opt.* 17, 3948-3958 (1978).

20. M. Niemz, "Thermal Interactions", Chap. 3 in *Laser-Tissue Interactions: Fundamentals and Applications*, pp. 68-75, Springer-Verlag, Berlin (2002).

21. H. S. Carslaw and J. C. Jaeger, *Conduction of heat in solids*, Clarendon Press, Oxford, UK (1959).

22. R. D. Peters, R. S. Hinks, and R. M. Henkelman, "Ex vivo tissue-type independence in proton-resonance frequency shift MR thermometry", *Mag. Res. Med.* 40 (3), 454-459 (1998).

23. J. F. Norfray, W. G. Klinger, I. A. Menon, S. Persad, P. A. Berger, and M. Ainscough, "A paramagnetic agent causing ochronotic arthropathy", *Invest. Radiol.* 23 (8), 609-615 (1988).

24. R. D. Peters, R. S. Hinks, and R. M. Henkelman, "Heat-source orientation and geometry dependence in proton-resonance frequency shift magnetic resonance thermometry", *Mag. Res. Med.* 41 (5), 909-918 (1999).

25. J. C. Chen, J. A. Moriarty, J. A. Derbyshire, R. D. Peters, J. Trachtenberg, S. D. Bell, J. Doyle, R. Arrelano, G. A. Wright, R. M. Henkelman, R. S. Hinks, S. Y. Lok, A. Toi, and W. Kucharczyk, "Prostate cancer: MR imaging and thermometry during microwave thermal ablation-initial experience", *Radiology* 214 (1), 290-297 (2000).

26. N. R. Miller, "Anatomy and Electrophysiology of the Retina", Chap. 2 in *Walsh and Hoyt's Clinical Neuro-Ophthalmology*, pp. 30-32, Williams & Wilkins, Baltimore, MD (1982).

27. Steven L. Jacques, Randolph D. Glickman, Jon A. Schwartz "Internal absorption coefficient and threshold for pulsed disruption of melanosomes isolated from retinal pigmented epithelium" *SPIE* Vol. 2681, P.468, (1996).

28. R. D. Peters, E. Chan, J. Trachtenberg, S. Jothy, L. Kapusta, W. Kucharczyk, and R. M. Henkelman, "Magnetic resonance thermometry for predicting thermal damage: an application of interstitial laser coagulation in an in vivo canine prostate model", *Mag. Res. Med.* 44 (6), 873-883 (2000).

29. T. J. White, M. A. Mainster, J. H. Tips, P. W. Wilson, "Chorioretinal thermal behavior", *Bull. Math. Biophys.* 32(3), 315-322 (1970).

30. C. R. Thompson, B. S. Gerstman, S. L. Jacques, M. E. Rogers, "Melanin granule model for laser-induced thermal damage in the retina", *Bull. Math. Biol.* 58, 513-553 (1996).

APPENDIX

Grant Identification: AFOSR F49620 -01-1-0211

Period of Grant: 1 Apr 2001 to 14 July 2004 (including no-cost extension from 1 Apr 2004 to 14 Jul 2004)

Scientific personnel supported by AFOSR:

Randolph D. Glickman, Ph.D. (Faculty, P.I.) 20% effort on project
Neeru Kumar, M.S. (Senior Research Assistant) 100% on project
Saher Maswadi, Ph.D. (Postdoctoral Fellow) 100% on project

Manuscripts submitted/published:

Glickman RD. Phototoxicity to the retina: Mechanisms of damage. International Journal of Toxicology, 21:473-490, 2002.

Glickman RD, Noojin GD, Stolarski DJ, Denton ML, Rockwell BA. Laser bioeffects associated with ultrafast lasers: Role of multiphoton absorption. In: Laser Bioeffects Meeting Proceedings, Courant D, Hugon M, and Andrieux M, Eds., Service de Santé des Armées, Paris, France, pp 6-1 - 6-13, 2002.

Glickman RD. Composition of the excimer laser-induced plume produced during LASIK refractive surgery. In Ophthalmic Technologies, Manns F, Soederberg PG, Ho A, Proc SPIE 4951, pp 124-132 (2003).

Glickman RD, Kumar N, Rockwell BA, Noojin GD, Denton ML, Stolarski DJ. Melanin and the cellular effects of ultrashort pulse, near infrared laser radiation. In Laser-Tissue Interaction XIV: Photochemical, Photothermal, and Photomechanical, Jacques SL, Duncan DD, Kirkpatrick SJ, Eds., Proc. SPIE 4961, pp 97-105 (2003).

Rowe-Rendleman C, Glickman RD. Possible therapy for age-related macular degeneration using human telomerase. Brain Res. Bull. 62:549-553, 2004.

Maswadi SM, Dodd DJ, Gao J-H, Glickman RD. Temperature mapping of laser-induced hyperthermia in an ocular phantom using magnetic resonance thermography. J. Biomed. Opt. 9:711-718, 2004.

Maswadi SM, Glickman RD, Dodd SJ, Gao JH. Non-invasive thermography of laser-induced hyperthermia using magnetic resonance. In: Laser Interaction with Tissue and Cells XV, Jacques

SL, Roach WP, Eds., Proc. SPIE 5319, pp 301-312, 2004.
Glickman RD and Johnson TE. Multiphoton absorption is probably not the primary threshold damage mechanism for femtosecond laser pulse exposures in the retinal pigment epithelium. In: Laser Interaction with Tissue and Cells XV, Jacques SL, Roach WP, Eds, Proc. SPIE, pp 162-172, 2004.

Denton ML, Eikum DM, Noojin GD, Stolarski DJ, Glickman RD, Rockwell BA. Photo-oxidation from mode-locked laser exposure to hTERT-RPE1 cells. In: Laser Interaction with Tissue and Cells XV, Jacques SL, Roach WP, Eds., Proc. SPIE 5319, pp 231-237, 2004.

Melendez RF, Kumar N, Maswadi SM, Zaslow K, Glickman RD. Photodynamic actions of indocyanine green and trypan blue on human lens epithelial cells in vitro. In press, Am. J. Ophthalmology, 2005.

Denton ML, Eikum DM, Noojin GD, Stolarski DJ, Glickman RD, Thomas RJ, Rockwell BA. A comparison of damage thresholds for continuous wave and femtosecond mode-locked lasers using an artificially pigmented RPE cell culture system. 2005, submitted to Nature.

Glickman RD, Natarajan M, Rockwell BA, Denton M, Maswadi SM, Kumar N, Nieves-Roldan F. Intracellular signaling mechanisms responsive to laser-induced photochemical and thermal stress. In: Laser Interaction with Tissue and Cells XVI, Proc. SPIE 5695, 2005, in press.

Inventions/Patents/Discoveries

None related to work supported by this grant.

Collaborators/Consultants:

Dr. Michael Denton. Dr. Denton is a scientist with the Northrup Grumman Information Technology group associated with the US Air Force Laser Lab at Brooks City Base (AL/HEDO), and also an AFOSR-supported researcher. Dr. Denton and I have collaborating on experiments using various retinal pigment epithelium (RPE) cell culture to investigate the bioeffects of ultrashort pulse laser. Using the dihydrodichlorofluorescein (DCFH) assay for reactive oxygen species that I developed in collaboration with Dr. Rockwell several years ago during an AFOSR-supported summer faculty research project, Dr. Denton has determined thresholds for photo-oxidative stress in cells exposed to various laser pulse widths. This work is the subject of a manuscript submitted to the journal Nature. Dr. Denton's contributions are included in Section One and Two of this report.

Dr. Jia-Hia Gao. Dr. Gao is a faculty member in the Department of Radiology at the University of Texas Health Science Center at San Antonio, and the magnetic resonance physicist at the

Research Imaging Center at this institution. Together with Dr. Saher Maswadi, the AFOSR-supported postdoctoral fellow in my laboratory, we have implemented a non-invasive method for measuring absolute and relative temperatures in tissue during laser exposure. This method was used to validate a heat-diffusion model for predicting laser-induced thermal changes, developed by Dr. Maswadi. The findings of our initial study are the subject of a manuscript published in the Journal of Biomedical Optics, and has been presented at the 2004 SPIE Biomedical Optics meeting, as well as the ARVO meeting in Ft. Lauderdale. The contributions of Dr Gao, as well as those of Dr. Maswadi, are included in Section Three of this report.

Dr. Thomas Johnson. Dr. Johnson is a faculty member at the Uniformed Services University of the Health Sciences (Bethesda, MD), and an AFOSR-supported researcher. Dr. Johnson and I have collaborated in order to assess the theoretical interaction of multiphoton absorption and the specific cellular targets. We presented the first part of our findings at the 2004 SPIE Biomedical Optics meeting in San Jose, and are planning a more detailed publication of this work thereafter. Dr. Johnson contributed to Section One of this report.

Dr. Mohan Natarajan. Dr. Natarajan is a faculty member of the Department of Radiation Oncology at the University of Texas Health Science Center at San Antonio. Dr. Natarajan is an AFOSR-supported researcher in the area of radio frequency radiation bioeffects. Dr. Natarajan and I both are interested in the production of oxidative damage in cells by non-ionizing radiation, and have looked for common endpoints produced by RF and laser radiation. Our initial experiments together have produced positive findings, using nuclear translocation of NF-kB as the endpoint. These findings were presented at the 2002 Oxygen Society meeting, and at the 2004 ARVO meeting. Dr. Natarajan's contributions are included in Section Two of this report. We are currently performing additional experiments to determine the dose-response of the NF-kB response, in order to complete the study for publication.

Dr. Benjamin Rockwell. Dr. Rockwell is a Senior Research Biophysicist at Brooks City Base (AFRL/HEDO), and directs the Ultrashort Pulse Laser Research program there. I have collaborated with Ben for many years. He and the Brooks City Base group have been instrumental in helping me design and carry out the current research program investigating the role of multiphoton absorption in photo-oxidative stress, in terms of providing access to the laser sources and optical detection facilities in his laboratory, and in helping to interpret the findings. His contributions are included in Sections One and Two of this report. We are continuing to correlate specific cellular endpoints with laser exposure characteristics.

Honors or Awards:

Randolph D. Glickman, Ph.D., was promoted to full professor with tenure at the University of Texas Health Science Center, as of 1 Sept 2004.

REPORT DOCUMENTATION PAGE

AFRL-SR-AR-TR-05-

0142

1. REPORT DATE *(DD-MM-YYYY)*	2. REPORT TYPE	3. DATES COVERED *(From - To)*
25-03-2005	Final	1 Apr 2001 to 14 Jul 2004

4. TITLE AND SUBTITLE
Laser bioeffects resulting from nonlinear interactions of ultrashort pulses with biological systems

5a. CONTRACT NUMBER

5b. GRANT NUMBER
AFOSR F49620-01-1-0211

5c. PROGRAM ELEMENT NUMBER

6. AUTHOR(S)
Glickman, Randolph D., Ph.D.

5d. PROJECT NUMBER

5e. TASK NUMBER

5f. WORK UNIT NUMBER

7. PERFORMING ORGANIZATION NAME(S) AND ADDRESS(ES)
Department of Ophthalmology
University of Texas Health Science Center
7703 Floyd Curl Drive
San Antonio, Texas 78229-3900

8. PERFORMING ORGANIZATION REPORT NUMBER
UTHSCSA-OPH-01-05

9. SPONSORING/MONITORING AGENCY NAME(S) AND ADDRESS(ES)
Air Force Office of Scientific Research
Directorate of Chemistry and Life Sciences
4015 Wilson Blvd., Rm. 713
Arlington, VA 22203

NL

10. SPONSOR/MONITOR'S ACRONYM(S)
AFOSR/NL

11. SPONSOR/MONITOR'S REPORT NUMBER(S)

12. DISTRIBUTION/AVAILABILITY STATEMENT
Approved for public release; distribution unlimited.

13. SUPPLEMENTARY NOTES

14. ABSTRACT
The role of multiphoton absorption in tissue damage induced by ultrashort pulse laser exposures was evaluated in a line of human-derived cells from the retinal pigment epithelium (RPE). DNA breakage in the cells was assessed with single cell gel electrophoresis ("comet" assay) following 250 fs or CW infrared (810 nm) laser. The near equivalence of DNA breakage in the RPE cells exposed to ultrashort and CW laser indicated that multiphoton absorption is not a major contributor to the ultrashort pulse laser damage threshold in the near infrared, but is likely to contribute to suprathreshold tissue damage. Another line of investigation of this project found that the transcription factor NF-kB was activated by visible laser exposure, apparently due to the absorption of laser energy in the melanin granules of the RPE cells. In addition, the temperature dependence of the proton resonance frequency (PRF) was utilized to measure laser-induced temperature gradients in tissue phantoms with magnetic resonance thermography. These measured gradients closely followed the spatiotemporal temperature distributions predicted by classical heat diffusion theory.

15. SUBJECT TERMS
Antioxidants, Comet assay, Damage threshold, DNA breakage, Hyperthermia, Infrared, Magnetic resonance thermography, Multiphoton absorption, NF-kB, Retinal Pigment Epithelium, Thermal model, Transcription factor, Ultrashort pulse laser,

16. SECURITY CLASSIFICATION OF:			17. LIMITATION OF ABSTRACT	18. NUMBER OF PAGES	19a. NAME OF RESPONSIBLE PERSON
a. REPORT	b. ABSTRACT	c. THIS PAGE			Glickman, Randolph D., Ph.D.
U	U	U	UU	65	19b. TELEPHONE NUMBER *(Include area code)* 210-567-8420